Cost-Effective Dyes Based on Low-Cost Donors and Pd-Free Synthesis for Dye-Sensitized Solar Cells

Artit Jarusarunchai, Arivazhagan Valluvar Oli, Aruna Ivaturi, and Neil Robertson*

The structural design of photosensitizers for dye-sensitized solar cells (DSSCs) usually involves modification of the donor and π-spacer moieties using expensive Pd crosscoupling reactions. Herein, the concept of more sustainable and cost-effective dyes to realize large-scale production is presented. Two dyes, coded BzC and PTZC, with low-cost donors, phenyl and phenothiazine, respectively, and 4H-cyclopenta [2,1-b:3,4-b']dithiophene π-spacer, are synthesized by Pd-free reactions, including Horner–Wadsworth–Emmons, with high overall yield (68% for BzC and 55% for PTZC). The best photovoltaic performances exhibit 3.00% and 5.92% together with relatively low ideality factor of 1.03 and 1.12 for BzC and PTZC, respectively, indicating efficient retardation of electron recombination from surface trap states. Finally, the synthesis costs for BzC and PTZC are estimated to be about 7.5–9 times lower than that of LEG-4 (as a commercial reference dye). The cost performances of BzC and PTZC are estimated to be around 5 times better than that of LEG-4.

1. Introduction

Renewable solar energy has attracted much attention and is an essential alternative energy supply to address the increasing energy demand and environmental concerns. In this aspect, photovoltaic (PV) technology is a good candidate for utilization of solar energy. One of the promising emerging PV technologies is dye-sensitized solar cells (DSSCs), where dye molecules, so-called photosensitizers, are used as the light absorber. In this regard, dyes can be considered among the most important components in DSSCs. The very first dyes used for high-performance DSSCs were based on Ru–polypyridyl complexes.[1–4] However, they usually show relatively low extinction coefficient and involve difficult synthesis and purification steps.[5] Thus, a new group of dyes called metal-free organic dyes subsequently emerged for DSSC applications. The organic dyes provide high extinction coefficient and flexibility in design and tuning of their electronic properties.[6] The structures of organic dyes are usually based on the state-of-the-art donor–π–acceptor (D–π–A) design. Unlike Ru–polypyridyl complexes whose excitation process is based on metal-to-ligand charge transfer (MLCT), the relevant electronic transition upon photoexcitation in the organic dyes is intramolecular charge transfer (ICT).[7] The electron density moves from the donor part to the acceptor part, leading to efficient charge separation.

A great deal of research in DSSCs has focused on the dye design and modification to tune the dye properties. In general, the structures of organic dyes usually contain a large extended conjugated system from the donor and π-spacer units to give broad and intense spectral absorption in visible light. The molecular design for the organic dyes normally relies on linking conjugated units via C—C or C—N bond formation. The reactions involved inevitably are Pd cross-coupling reactions, such as the Suzuki–Miyaura, Stille, and Buchwald–Hartwig reactions. These reactions involve the use of Pd-based catalysts including a specific coupling partner, for example, organoborons for the Suzuki–Miyaura reaction and organostannanes for the Stille reaction. Notwithstanding their versatility, the Pd catalysts are normally expensive as Pd is a rare metal and they need additional ligands added to perform the catalysis. The high cost of the catalysts can increase the total cost of dye synthesis, making the dyes more expensive. Moreover, some starting materials, such as organostannanes, cause toxicity concerns and possible tin contamination in the products.[8] The organostannanes have been acknowledged to cause toxicity to a range of neurological and liver systems.[9] Therefore, more sustainable alternative reactions must be sought to address the toxicity concerns and lower the cost of dye production. One of the promising alternative reactions is the Wittig or Horner–Wadsworth–Emmons (HWE) reaction.

As mentioned earlier, the organic dye architecture is based on D–π–A design and the modification of the dye structure is normally carried out by changing the donor and π-linker to tune the properties. One of the most commonly used materials for the donor part in the organic dyes is the derivatized triarylamine unit due to its electron donor capability.[10] To further improve the donor moiety, many modifications on the triarylamine-based donor are usually carried out, such as the addition of alkyl chains[11–14] or further extending the conjugation lengths.[15–17]

A. Jarusarunchai, N. Robertson
School of Chemistry
University of Edinburgh
Edinburgh EH9 3FJ, UK
E-mail: neil.robertson@ed.ac.uk

A. Valluvar Oli, A. Ivaturi
Smart Materials Research and Device Technology (SMaRDT) Group
Department of Pure and Applied Chemistry
University of Strathclyde
Glasgow G1 1XL, UK

The ORCID identification number(s) for the author(s) of this article can be found under https://doi.org/10.1002/solr.202200375.
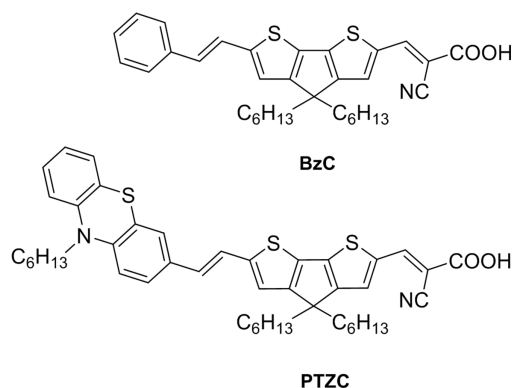
Figure 1. **BzC** and **PTZC** molecular structures.

These modifications, however, increase the costs associated with the already high synthesis cost of the organic dyes.

Phenothiazine (PTZ) has also been used in DSSCs due to its electron donor capability, low cost, and butterfly conformation which prevent molecular aggregation.[18,19] Buene et al. studied the effect of various auxiliary donors connected to PTZ-donor and thiophene as π-spacer to achieve D′–D–π–A structure.[20] The power conversion efficiency (PCE) of auxiliary donor-incorporated dyes was enhanced by moderate 4–11% relative improvement. This highlights that the auxiliary donor may not be necessary for PTZ-based dyes. Moreover, PTZ-based dyes with various π-spacers, such as thiophene,[19–21] furan,[19] 3,4-ethylenedioxy thiophene (EDOT),[19,22] phenyl,[23] and 4H-cyclopenta[2,1-b:3,4-b']dithiophene (CPDT),[24] for DSSCs have been investigated. Out of these π-spacers, CPDT possesses large conjugation and ease of structural modification, such as introduction of alkyl chains. Marszalek et al. synthesized the dye which has PTZ as electron donor connected to CPDT π-spacers by Pd crosscoupling reaction to form direct C—C bond between PTZ and CPDT.[21] However, as mentioned earlier, alternative and cost-effective reactions for connecting donor and π-spacers units are beneficial for sustainable dye synthesis and large-scale production.

In this work, we designed and synthesized two new dyes, **BzC** and **PTZC** (**Figure 1**), which do not involve Pd cross-coupling reaction. The reaction used to connect the donor and π-spacer was based on the Horner-Wadsworth-Emmons (HWE) reaction. Moreover, low-cost PTZ and phenyl moieties were used as the donor to further lower the synthesis cost. PTZ also possesses electron-donor ability[18] in which we expect it can substitute the triarylamine-based moiety leading to lower synthesis cost. The use of phenyl ring as the donor in **BzC** is for a control dye structure so as to compare the effect of the donor group within this dye design. For π-spacer, commonly used CPDT was chosen due to its facile modifications, such as introduction of long alkyl chains, and large conjugation. To demonstrate the low synthesis cost, estimation was made not only for the synthesis costs but also for the cost performance per cm^2 per %PCE of these two dyes in comparison with highly efficient commercial dye **LEG-4**.

2. Results and Discussion

2.1. Synthesis

BzC was synthesized according to **Scheme 1**. CPDT was first alkylated with hexyl chains to give compound **1** which subsequently underwent the Vilsmeier–Haack reaction to yield compound **2**. To achieve a conjugated structure suitable for a dye, CPDT unit was joint to the phenyl ring by a double bond using the HWE reaction. Benzyl bromide was changed to compound **3** by the Michaelis–Arbuzov reaction using triethyl phosphite (P(OEt)$_3$). After that, compound **3** and compound **2** underwent the HWE reaction to give compound **4**. The Vilsmeier–Haack reaction was performed again with compound **4** to synthesize compound **5** which was subsequently transformed into **BzC** by the Knoevenagel condensation with cyanoacetic acid catalyzed by piperidine, yielding a pink solid **BzC** with the overall yield of 68.5%.

Scheme 2 shows the synthesis procedure of **PTZC** which started with the N-alkylation of PTZ with hexyl bromide giving compound **6**. The Vilsmeier–Haack reaction was used to formylate compound **6** to give compound **7**. The formyl group in
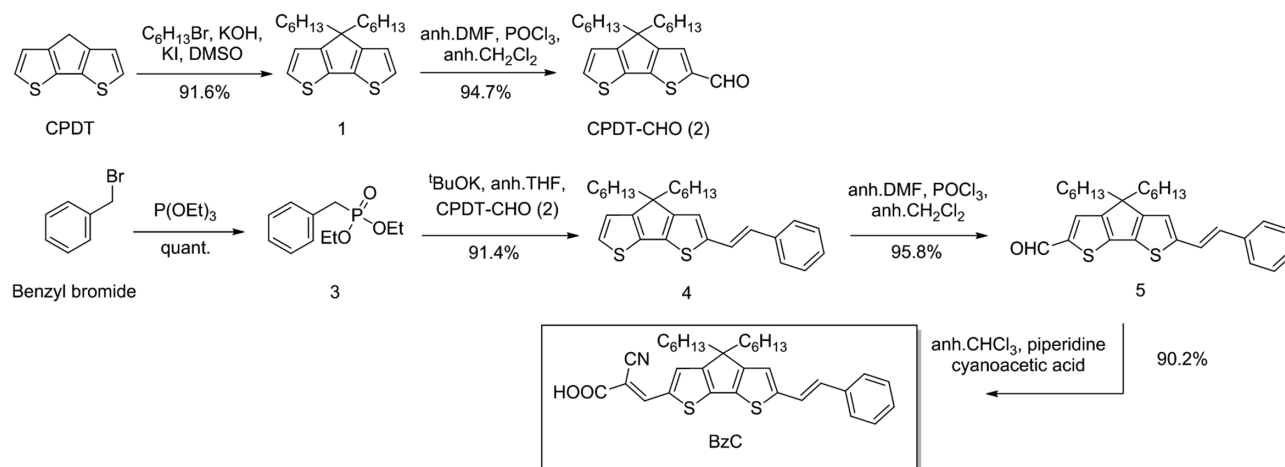
Scheme 1. Synthetic method of **BzC**.
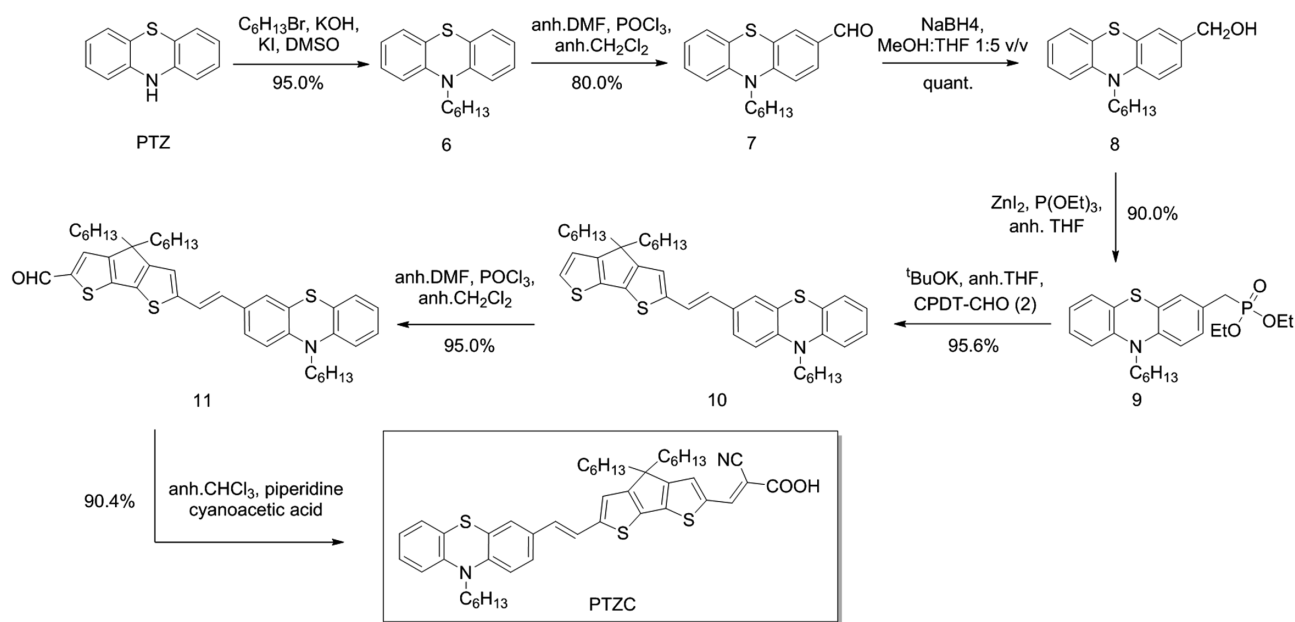
Scheme 2. Synthetic method of **PTZC**.

compound **7** was reduced by NaBH$_4$ to yield compound **8**. We first tried the Wittig reaction to connect alkylated PTZ with compound **2** via double bond, as shown in Scheme S1, Supporting Information. This method has been used to connect PTZ and the π-spacer with a double bond in previous literature[21–23,25,26] for DSSC applications. However, it leads to a mixture of (E)- and (Z)-isomers in which the (E)-isomer is the major product (around 80%) as seen from ^{1}H NMR spectrum of compound **10** in Figure S1, Supporting Information. To convert the (Z)-isomer into (E)-isomer, isomerization of the mixture of isomers with a catalytic amount of iodine is often carried out. However, this treatment leads to more synthetic steps and gives relatively low yield.[23,25] The isomerization reaction can be avoided using the HWE reaction instead of the Wittig reaction. To perform the HWE reaction, a conversion of compound **8** to **9** was necessary which can be done by the Michaelis–Arbuzov reaction via **PTZ–CH₂Br**. The attempts to convert compound **8** to **PTZ–CH₂Br** as shown in Scheme S2, Supporting Information, by either reacting with PBr$_3$ or the Appel reaction (with CBr$_4$ and triphenylphosphine) were unsuccessful. This may be due to the instability of the intermediate or **PTZ–CH₂Br**. To solve the problem of the unsuccessful attempts to prepare **PTZ–CH₂Br**, a direct conversion[27] from compound **8** to compound **9** using ZnI$_2$ and P(OEt)$_3$ was successfully performed, as shown in Scheme 2. After obtaining compound **9**, it underwent the HWE reaction with compound **2** to yield compound **10**, as shown in Scheme 2. The Vilsmeier–Haack reaction was performed on compound **10** giving compound **11**. The final dye **PTZC** was synthesized by the Knoevenagel condensation reaction of compound **11** with cyanoacetic acid and piperidine as the catalyst, giving rise to a purple solid of **PTZC** with the overall yield of 55.6%. To the best of our knowledge, compound **9** in Scheme 2 is novel and can be prepared easily by the direct conversion from its alcohol counterpart. This can open up a new way to synthesize bulky

PTZ-bearing phosphonate reagents which may be widely used for the HWE reaction, avoiding the formation of isomers.

2.2. Photophysical and Electrochemical Properties

The UV–vis absorption and normalized emission spectra of **BzC** and **PTZC** in DCM are presented in **Figure 2**A. Their corresponding results are shown in **Table 1**. **BzC** and **PTZC** exhibit a prominent peak in the visible region. **BzC** shows the maximum absorption (λ_{max}) and extinction coefficient of 523 nm and 58 500 M^{-1}cm^{-1}, respectively, while **PTZC** exhibits λ_{max} at 547 nm, which has a bathochromic shift of 838 cm^{-1} compared with **BzC**, with extinction coefficient of 63 000 M^{-1}cm^{-1}. These prominent peaks (λ_{max}) are ascribed to an ICT process. The bathochromic shift of **PTZC** reflects the larger conjugation of the PTZ unit compared with the phenyl ring, leading to a smaller optical gap. It is worth mentioning that their extinction coefficient values are astonishingly high with such simple dye structures. The high extinction coefficients may be due to the fact that their structure is highly conjugated because of the planar structure due to the double bond as well as the CPDT unit which facilitates ICT process. For the photoluminescent results of **BzC** and **PTZC** in DCM (Figure 2A, S2, Supporting Information and Table 1), **BzC** shows the emission peak maximum (λ_{em}) at 589 nm with Stokes shift of 2142 cm^{-1}, whereas λ_{em} of **PTZC** is observed at 624 nm with Stokes shift of 2256 cm^{-1}. Moreover, the emission peak of **PTZC** exhibits a small shoulder around 650 nm, which is not seen for **BzC**. The larger Stokes shift and small shoulder of **PTZC** may imply that **PTZC** experiences different processes of structural reorganization during the electronic transition.[28] As shown in Figure 2A, the intersection point of the absorption and emission spectra can be used to estimate the optical gaps (E_{0-0}) of **BzC** and **PTZC**, which are 2.23 and 2.10 eV for **BzC** and **PTZC**, respectively.
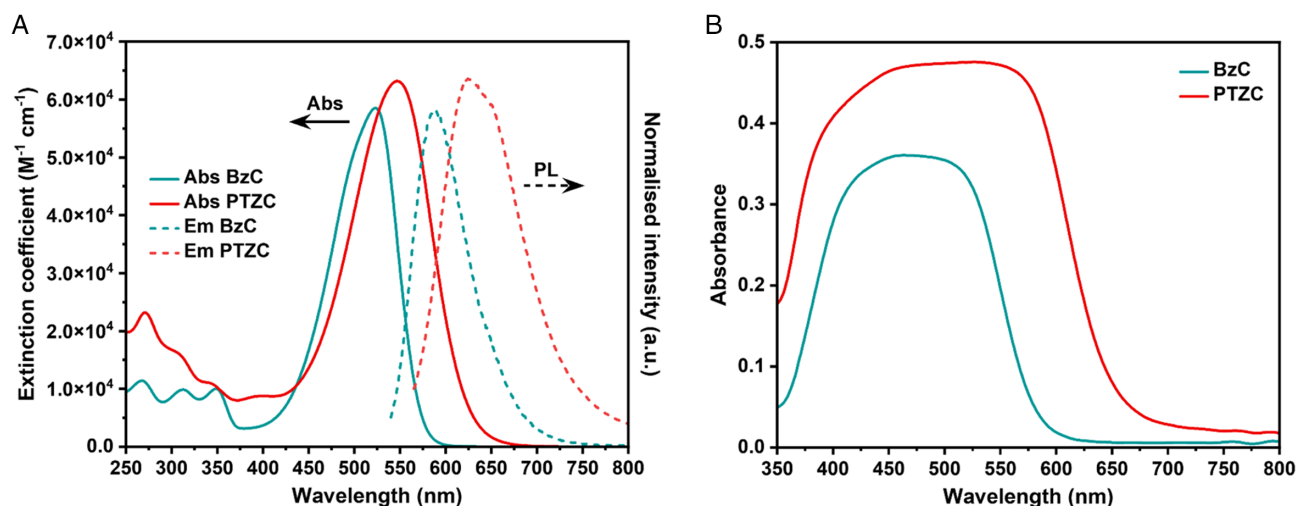
Figure 2. A) UV–vis spectra and normalized emission spectra of **BzC** and **PTZC** in DCM and B) UV–vis absorption spectra of **BzC** and **PTZC** on transparent TiO₂.

Table 1. Photophysical and electrochemical properties of **BzC** and **PTZC**.

Dye	λ_{max} [nm], ε [M^{-1} cm^{-1}]	λ_{em} [nm]	E_{gap}^{opt} [eV][a]	E_{ox} versus NHE [V][b]	E_{red} versus NHE [V][b]	E_{HOMO} [V][c]	E_{LUMO} [V][c]	E_{ox}^{*} [V][d]
BzC	523, 59 000	589	2.23	1.20	−1.42	−5.37	−2.75	−1.03
PTZC	547, 63 000	624	2.10	0.85	−1.41	−5.02	−2.76	−1.25

[a]The optical gap (E_{0-0}) was determined by the intersection point of normalized absorbance and emission in DCM. [b]Potentials were measured in DCM with 0.3 M TBAPF₆ as a supporting electrolyte versus Fc/Fc⁺ and were converted to be against NHE by addition of 0.63 V.[59] [c]The HOMO and LUMO energies were estimated by: $E_{HOMO(LUMO)} = -4.8 - (E_{ox(red)}$ vs Fc/Fc⁺).[60] [d]Excited-state oxidation potential (E_{ox}^{*}) was determined by $E_{ox} - E_{gap}^{opt}$.

The spectral response of **BzC** and **PTZC** adsorbed on the 4 µm-transparent TiO₂ film was determined by UV–vis absorption and the results are depicted in Figure 2B. When compared with the corresponding absorption spectra in DCM (Figure 2A), their spectral profiles on film become broader due to H-aggregates.[29] The broader spectral profile can benefit the light-harvesting efficiency. As shown in Figure 2B, the absorption from around 350 to 450 nm from both dyes improves significantly when compared with the corresponding absorption in DCM.

Cyclic voltammetry (CV) and square-wave voltammetry (SWV) were used to characterize the electrochemical properties of **BzC** and **PTZC**. Their CVs in positive potential range (Figure S3, Supporting Information) reveal that both **BzC** and **PTZC** show both forward and return waves, representing their chemical and electrochemical reversibility upon oxidation reaction. It is worth mentioning that although **BzC** shows incomplete chemical reversibility at slow scan rate (Figure S3, Supporting Information), this improves with increasing scan rate, confirming the chemical stability of **BzC** in the context of a DSSC photosensitizer, given that dye regeneration is usually in a microsecond timescale.

According to **Figure 3**A and Table 1, SWVs of **BzC** and **PTZC** show that the oxidation process of **BzC** occurs at 0.57 V against Fc/Fc⁺ or 1.20 V against normal hydrogen electrode (NHE), which is more positive than the first oxidation potential of **PTZC** (0.22 V against Fc/Fc⁺ or 0.85 V against NHE). Moreover, **PTZC** shows two oxidation processes within the potential range (from −1.70 to 1.35 V). The difference in oxidation potential between **BzC** and **PTZC** can be explained in terms of the difference in the donor group. The less-positive oxidation potential of **PTZC** is attributed to more extended conjugation of the PTZ unit than phenyl ring in **BzC**. In contrast to oxidation processes, the reduction processes of **BzC** and **PTZC** occur at similar potential (around −2.0 V against Fc/Fc⁺ or −1.4 V against NHE, Figure 3A and Table 1, respectively). The similar reduction potentials imply that the reduction process is attributed to cyanoacrylic acid.

The evaluation of the optical and electrochemical properties is crucial as they provide information about the driving force for dye regeneration, charge injection, and light-harvesting capability. Figure 3B illustrates a visual diagram of energy-level alignment of TiO₂/dye/electrolyte (I⁻/I₃⁻). It is clearly seen that the oxidation potentials of **BzC** and **PTZC** are well below the redox potential of I⁻/I₃⁻ (0.35 V vs NHE),[30] which indicates favorable driving force for dye regeneration. When compared with the conduction band edge energy level (E_{CB}) of TiO₂, the excited oxidation potential (E_{ox}^{*}) values of the dye molecules are higher than E_{CB} of TiO₂ (−0.5 V vs NHE),[30] confirming sufficient driving force for electron injection to the conduction band of TiO₂.

2.3. Computational Study

The frontier molecular orbitals and electronic energy level of **BzC** and **PTZC** in DCM solvation model were investigated by DFT calculations at B3LYP[31] level of theory with 6-31G(d) basis set. To ensure that all optimization calculations were at local minima, frequency calculations were also performed together with optimization calculations. As shown in **Figure 4**, the HOMO
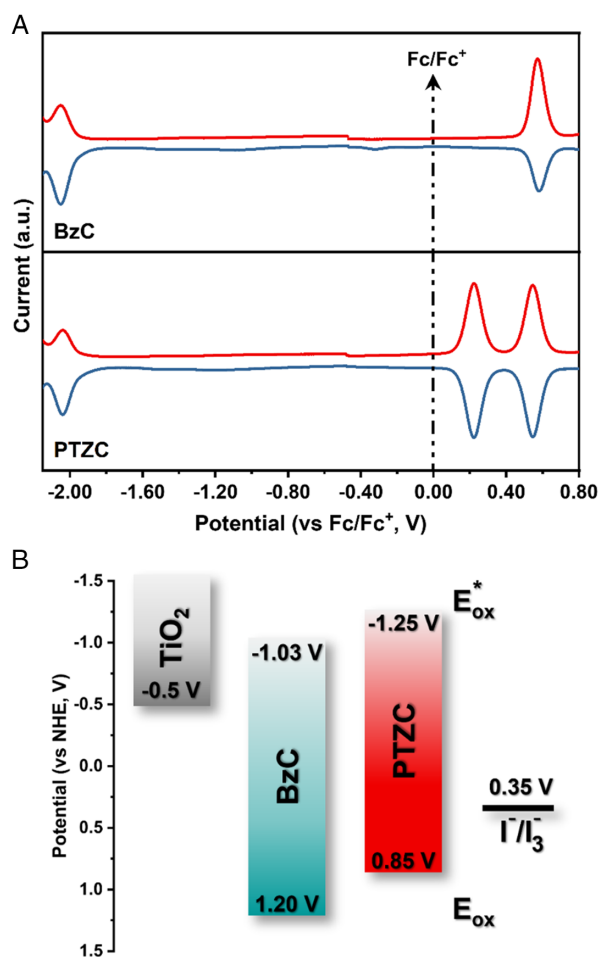
Figure 3. A) Square-wave voltammograms of **BzC** and **PTZC** in DCM and B) energy alignment of **BzC** and **PTZC** in comparison with TiO$_2$ and I$^-$/I$_3^-$ redox couple.

slightly underestimated, compared with experimental results. However, the trend of phenyl and PTZ units on absorption and extinction coefficient is in line with the experimental values, where **PTZC** exhibits bathochromic shift and higher extinction coefficient with respect to **BzC**. Table 2 also highlights the difference in the molecular orbital (MO) contributions to electronic transition at calculated λ_{max} of **BzC** and **PTZC** as well as oscillator strength (f). For **BzC**, the major %MO contribution to the transition at 491 nm (523 nm from experiment) originates from HOMO to LUMO, accounting for 93%. On the contrary, the major MO contributions to the transition at 517 nm (547 nm from experiment) for **PTZC** are attributed to a mixture of HOMO to LUMO and HOMO-1 to LUMO in which the former has a larger contribution of 74%. The oscillator strength is related to the probability of the transition from ground state to excited state[33] and is proportional to extinction coefficient.[34] As shown in Table 2, the oscillator strength of **PTZC** is larger than that of **BzC**, which indicates that the probability of the transition in **PTZC** is higher, and that contributes to higher extinction coefficient.

2.4. Photovoltaic Performance

Solar cells based on **BzC** and **PTZC** were fabricated with double-layer TiO$_2$ (4 μm transparent layer and 4 μm scattering layer) and I$^-$/I$_3^-$ electrolyte. The photovoltaic performances were measured under AM 1.5G simulated solar light (100 mW cm^{-2}). The corresponding results are shown in **Table 3**, and their champion current–voltage ($J–V$) curves are shown in **Figure 5**A. The devices with **LEG-4** were also fabricated for cost analysis discussion only and the results are tabulated in Table 3. From the results of **BzC** and **PTZC**, the best device with **BzC** exhibited short-circuit current density (J_{sc}), open-circuit voltage (V_{oc}), and fill factor (FF) of 7.88 mA cm^{-2}, 0.52 V, and 0.73, respectively, giving PCE of 3.00%, whereas the best device with **PTZC** achieved J_{sc}, V_{oc}, and FF of 12.92 mA cm^{-2}, 0.61 V, and 0.75, respectively, leading to PCE of 5.92%. It is clearly seen that the higher PCE obtained from **PTZC** is due to higher J_{sc} and V_{oc}.

To gain more insight into the photovoltaic performances, the incident photon-to-electron conversion efficiency (IPCE) measurements were carried out (Figure 5B). IPCE can be expressed in terms of light harvesting efficiency LHE(λ), injection efficiency (φ_{inj}), charge collection efficiency (η_{col}), and dye regeneration efficiency (φ_{reg}), as shown in Equation (1)[17]

$$IPCE = LHE(\lambda) \times \varphi_{inj} \times \varphi_{reg} \times \eta_{col} \qquad (1)$$

As mentioned earlier, E_{ox} of **BzC** and **PTZC** are more positive than the redox potential of I$^-$/I$_3^-$, which can ensure sufficient driving force for dye regeneration. When compared with the CB level of TiO$_2$, their E_{ox}^* are more negative, and the difference between E_{ox}^* and CB is greater than 0.2 V, which indicates that fast electron injection rate is possible.[35] Moreover, the E_{ox}^* of **PTZC** is more negative than that of **BzC**, reflecting larger driving force for electron injection. In terms of LHE, it can be expressed in relation with absorbance of the film (A_f) as shown in Equation (2).[36]

$$LHE(\lambda) = 1 - 10^{-A_f} \qquad (2)$$

of **BzC** is distributed across almost the entire structure. On the other hand, LUMO is localized on cyanoacrylic acid with a small contribution on the phenyl ring. Similarly, for **PTZC**, the HOMO is mostly located on PTZ with some extent on CPDT. The LUMO is shifted toward cyanoacrylic acid with negligible contribution from PTZ. By comparing the effect of substituents (phenyl and PTZ) on the HOMO–LUMO gap, the trend in which the HOMO energy is raised (less negative in vacuum scale) with more extended conjugation of PTZ corresponds to the experimental values (electrochemical results), whereas the LUMO energies are unaffected. As a result, the HOMO–LUMO gap is reduced upon more conjugation present in the structure.

To shed light on the spectroscopic properties of **BzC** and **PTZC**, the optimized geometry of **BzC** and **PTZC** was subjected to time-dependent DFT (TDDFT) calculations at CAM-B3LYP[32] level of theory with 6-31G(d) basis set in DCM solvation model. The experimental and calculated absorption spectra are shown in Figure S4, Supporting Information, and the corresponding transitions are summarized in **Table 2**. According to Figure S4, Supporting Information, the calculated spectra exhibit λ_{max} at 491 and 517 nm for **BzC** and **PTZC**, respectively, which are
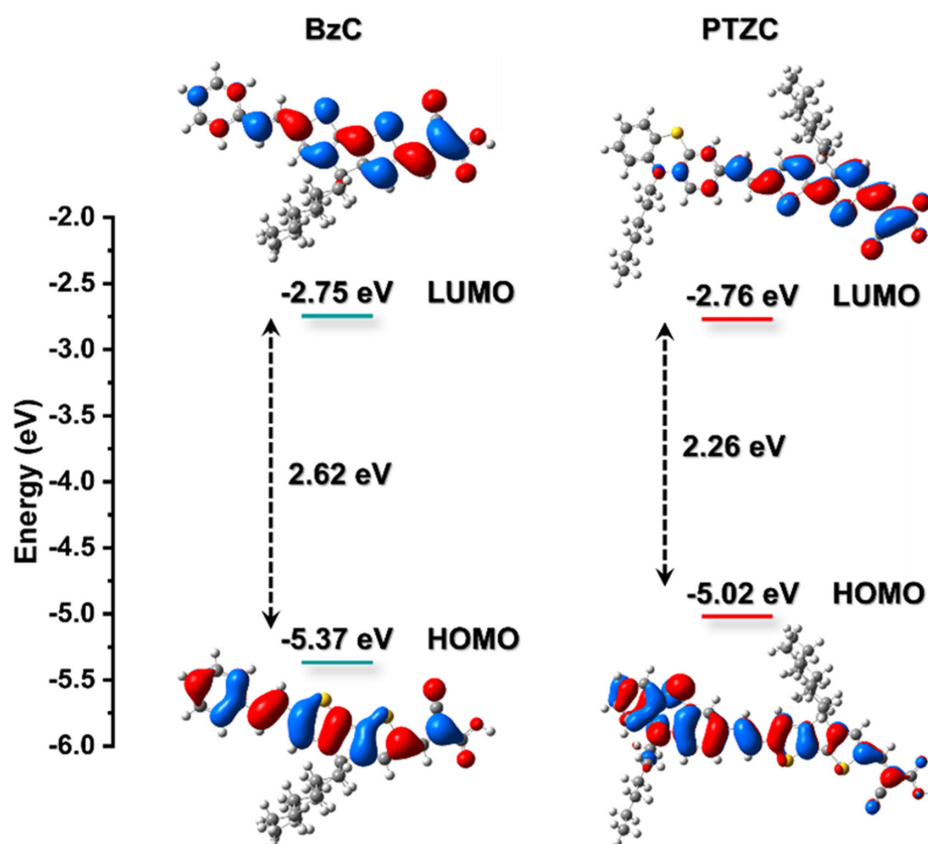
Figure 4. Calculated frontier molecular orbitals in DCM solvation model with experimental energy levels (Table 1) of **BzC** and **PTZC**.

Table 2. Calculated lowest electronic transition of **BzC** and **PTZC** with corresponding molecular orbital (MO) contribution and oscillator strength (f).

Dye	λ_{max} [nm]	%MO contribution	f
BzC	491	HOMO to LUMO (93%)	1.74
PTZC	517	HOMO to LUMO (74%)	2.62
		HOMO-1 to LUMO (18%)	

As shown in Figure 5B, **PTZC** exhibits broad IPCE spectrum ranging from 400 to 600 nm with the maximum IPCE around 75%. The onset of the IPCE of **PTZC** appears around 700 nm, which is consistent with the absorption spectrum. On the other hand, **BzC** shows much narrower IPCE spectrum with the maximum around 70% at 450 nm. This difference in IPCE profile between **BzC** and **PTZC** originates from their absorption properties in which **PTZC** exhibits higher extinction coefficient and broader absorption spectrum on transparent TiO$_2$ (Figure 2B). Apart from the absorption profiles, the amount of adsorbed dye on the TiO$_2$ surface also determines the LHE. The analysis of dye uptake by dye desorption reveals that the dye loading of **PTZC** is higher than that of **BzC** (Table 3). The combination between higher extinction coefficient, boarder absorption spectrum, and greater amount of adsorbed dye from **PTZC** leads to superior LHE. In terms of η_{col}, it can be determined by Equation (3).[7]

Table 3. Photovoltaic parameters of the champion solar cells based on **BzC** and **PTZC** with I$^-$/I$_3^-$ electrolyte under illumination with AM 1.5 G (100 mW cm^{-2}); with the average results calculated from six individual cells mentioned in brackets.

Dye	J_{sc} [mA cm^{-2}]	V_{oc} [V]	FF	PCE [%]	Dye loading [mol cm^{-2}]
BzC	7.88 (6.19 ± 0.98)	0.52 (0.48 ± 0.02)	0.73 (0.72 ± 0.02)	3.00 (2.16 ± 0.46)	1.78 × 10^{-7}
PTZC	12.92 (12.70 ± 0.29)	0.61 (0.60 ± 0.01)	0.75 (0.74 ± 0.01)	5.92 (5.66 ± 0.15)	2.11 × 10^{-7}
LEG-4[a]	15.41 (15.50 ± 0.26)	0.68 (0.67 ± 0.002)	0.71 (0.68 ± 0.05)	7.41 (7.10 ± 0.004)	1.22 × 10^{-7}

[a]**LEG-4** results given in brackets are averaged from three individual cells
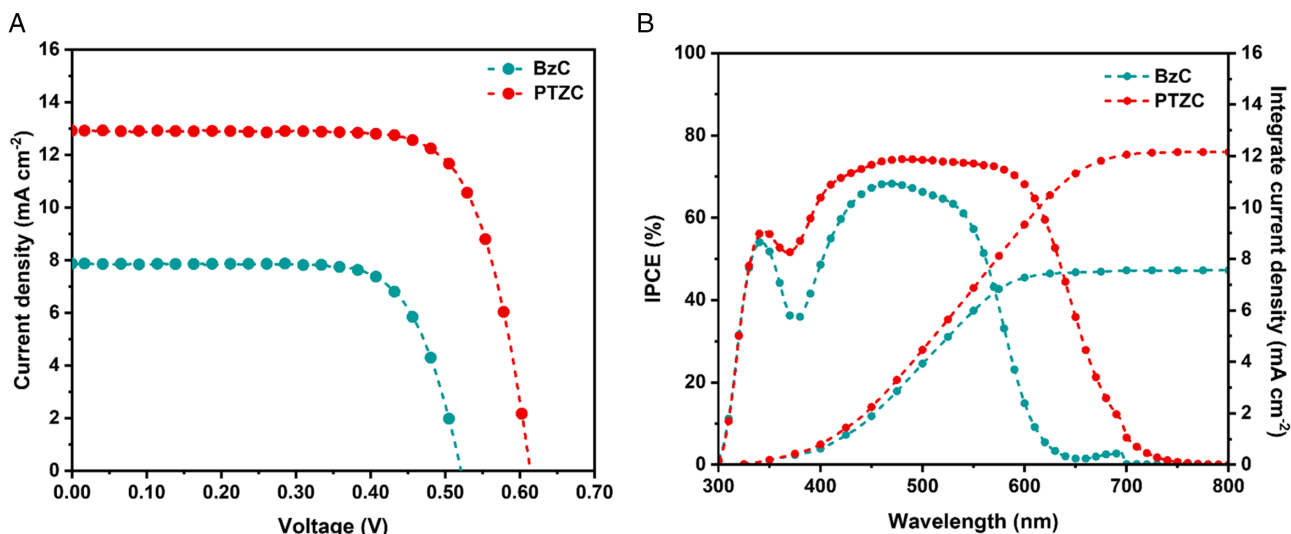
Figure 5. A) J–V curves for **BzC** and **PTZC** obtained for the best devices under illumination of AM 1.5G (100 mW cm^{-2}) and B) IPCE spectra of **BzC** and **PTZC** based solar cells with integrated current density.

$$\eta_{col} = \frac{1}{1 + \dfrac{\tau_t}{\tau_{rec}}}$$
$$\eta_{col} = \frac{1}{1 + \dfrac{R_t}{R_{rec}}} \qquad (3)$$

where R_t and R_{rec} are transport and recombination resistances, which can be obtained from electrochemical impedance spectroscopy (EIS) measurement. More details on the determination of these parameters can be found in the EIS section. The results show that **BzC** exhibits η_{col} around 95% which is higher than that of **PTZC** (around 88%). Nonetheless, the effect of higher η_{col} of **BzC** on IPCE is less pronounced than the better LHE of **PTZC**.

As a result, the overall parameters determining IPCE of **PTZC** are superior to those of **BzC**.

2.5. EIS Measurement

EIS is a powerful technique that can be used to analyze the processes governing the performance of DSSCs, especially V_{oc}. The EIS measurements were performed in the frequency range from 1 MHz to 0.1 Hz under white LED illumination at various forward biases. The results were fit using a transmission line model[37] and the equivalent circuit is depicted in Figure S5, Supporting Information. In general, the EIS spectra (**Figure 6**) show a typical DSSC feature with two semicircles where the first semicircle at high-frequency range represents Pt/electrolyte
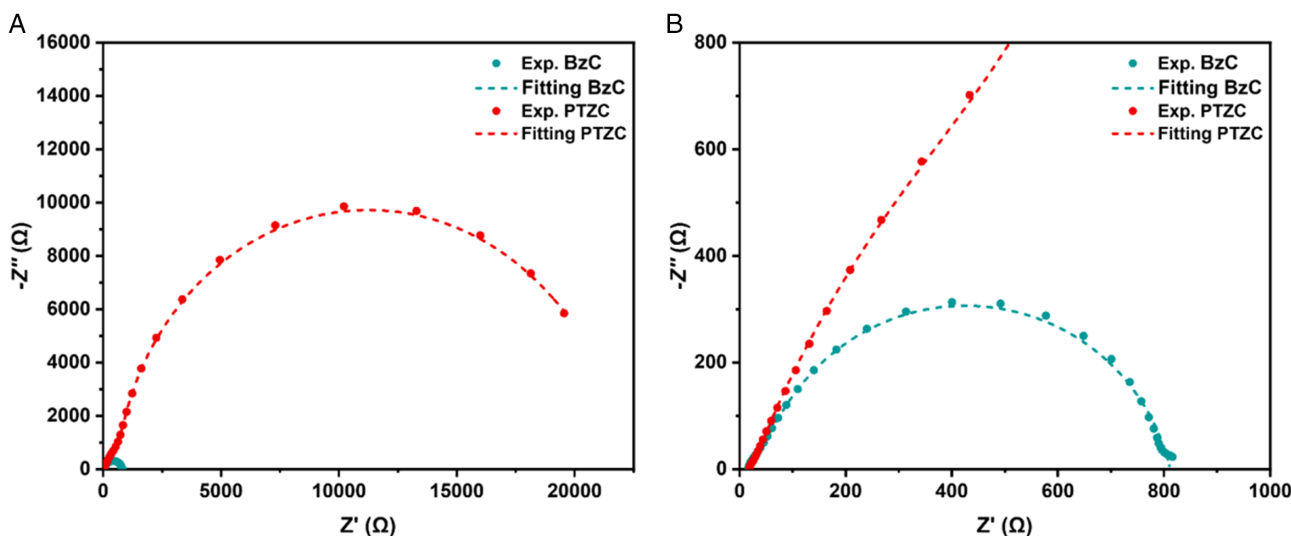

Figure 6. A) Nyquist plots of **BzC**- and **PTZC**-based solar cells measured under white LED illumination and forward bias of −0.42 V and B) enlarged Nyquist plots at the same forward bias.
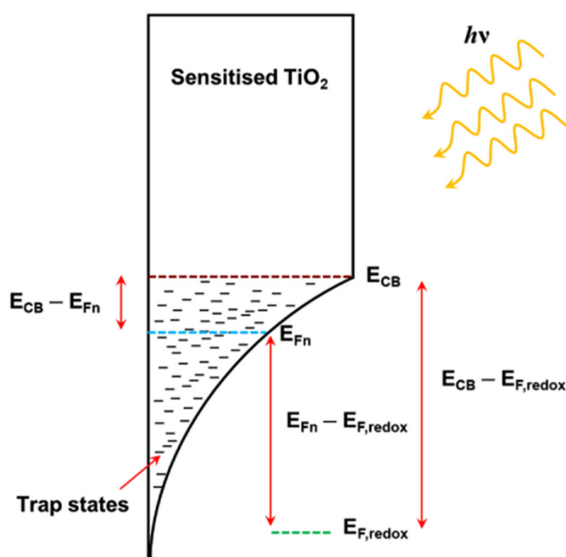
Figure 7. Graphical illustration of the photogenerated voltage of sensitized TiO_2 film under illumination.

interface and the second semicircle at intermediate-frequency range represents TiO_2/dye/electrolyte interface.[38] As shown in Figure 6B, the EIS spectrum of **BzC** also shows a minor feature of the third semicircle at low-frequency range which represents electrolyte diffusion.[38] However, due to an unclear semicircle, parameters related to electrolyte diffusion are omitted in the equivalent circuit. To represent the EIS spectra close to their respective V_{oc}, Figure S6, Supporting Information, shows the Nyquist plots at −0.48 V for **BzC** and at −0.56 V for **PTZC**.

As shown in J–V curve results, the difference in the dye structure also plays a role in V_{oc} determination in the full device. V_{oc} of the device is determined by the difference between quasi-Fermi level of TiO_2 (E_{Fn}) and the redox potential of electrolyte ($E_{F,redox}$) as depicted in **Figure 7** and described by Equation (4)[39]

$$V_{oc} = \frac{E_{Fn} - E_{F,redox}}{q} \tag{4}$$

where q is elementary charge. As the two devices were made with the same electrolyte (I^-/I_3^-), $E_{F,redox}$ is considered unchanged. Therefore, the difference in V_{oc} between the two devices stems from the variation of E_{Fn}. This alteration of E_{Fn} can be expressed by Equation (5).[39]

$$E_{Fn} = E_{CB} + k_B T \ln\left(\frac{n_c}{N_c}\right) \tag{5}$$

where E_{CB} is the conduction band edge of TiO_2, k_B is Boltzmann constant, T is temperature, n_c is the free carrier density, and N_c is the density of states in CB of TiO_2 taken as $7 \times 10^{20}\,cm^{-3}$.[40] Equation (5) implies that raising E_{CB} leads to an increase in E_{Fn}, hence, higher V_{oc}.

The parameters mentioned above are influenced by the dye properties. For example, some dyes can cause a large upward shift in E_{CB} which might lead to higher V_{oc}. Moreover, changing dye may influence the trap states[41] which, subsequently, impacts the performance of the devices. EIS measurement allows us to analyze these variables affected by dye through fitted EIS parameters, such as transport resistance (R_t), chemical capacitance (C_μ), and recombination resistance (R_{rec}). The following discussion will focus on each fitted parameter associated with the variable affected by dye properties.

The transport resistance (R_t) is one of the useful parameters extracted from EIS fitting with the equivalence circuit shown in Figure S5, Supporting Information. It provides information about E_{CB} and its relationship with voltage can be displayed in Equation (6)[42]

$$R_t = \frac{L}{A(1-p)q\mu_0 N_c} \exp\left[\frac{E_{CB} - E_{F,redox}}{k_B T}\right] \exp\left[-\frac{qV}{k_B T}\right]$$

$$R_t = R_{t0} \exp\left[-\frac{qV}{k_B T}\right] \tag{6}$$

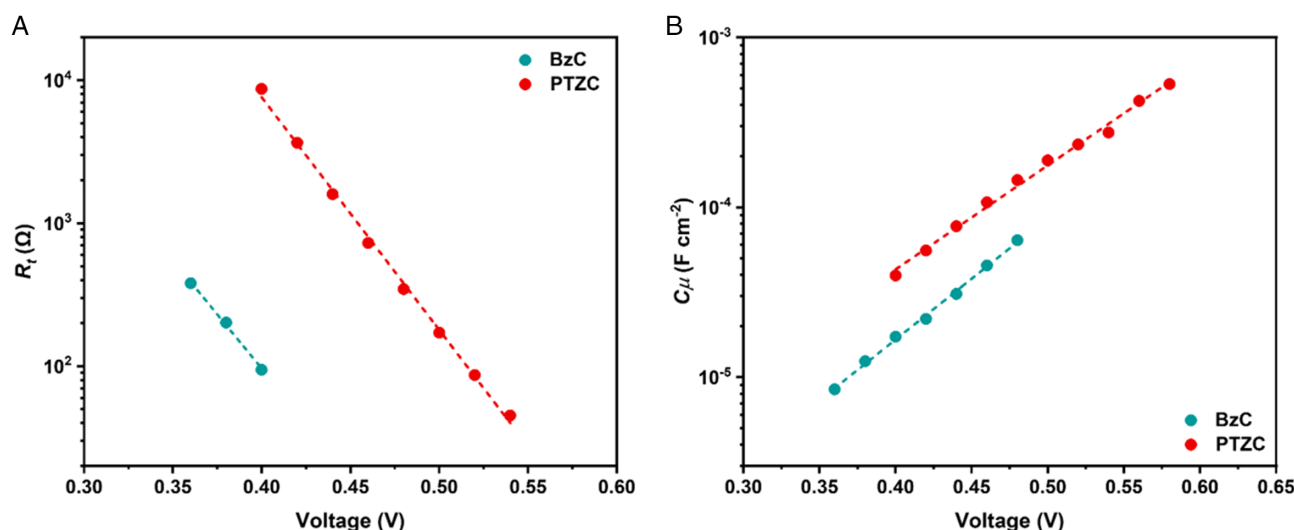
Figure 8. A) Transport resistance (R_t) as a function of applied bias where dotted lines show the fitting according to Equation (6) and B) chemical capacitance (C_μ) as a function of applied bias where dotted lines show the fitting according to Equation (7). The parameters used for fitting are obtained from EIS measurement with transmission line model at various applied forward bias.

Table 4. Parameters from fitted R_t, C_μ, and R_{rec} results, from fitting Equation (6), (7), and (9), respectively.

Dye	α	$E_{CB}-E_{F,redox}$ [eV]	N_t [cm^{-3}]	m
BzC	0.42	0.76	7.33×10^{18}	1.03
PTZC	0.36	0.90	6.69×10^{19}	1.12

where A denotes film area, L is the film thickness (8 μm), p is porosity taken as 0.6,[43] and μ_0 is electron mobility of TiO$_2$ taken as 4 cm^2 V^{-1} s^{-1}.[40] Fitting R_t as a function of voltage (**Figure 8**A) shows an exponential decrease in R_t with increasing voltage. Figure 8A indicates that **PTZC** shows a positive shift in voltage around 100 mV with respect to **BzC**. Assuming that A, L, μ_0, and N_c are identical across the devices,[37,42] this positive shift implies the upward displacement of E_{CB} in the case of **PTZC**. To give quantitative estimation of E_{CB} of **BzC** and **PTZC**, which is explained in terms of $E_{CB}-E_{F,redox}$ (see Figure 7 for clarity), the intercepts from $\ln(R_t)$ versus V plot (Figure 8A and Equation (6)) were used, and the results are shown in **Table 4**. The trend in R_t is consistent with the results from the *J–V* curve measurement in which **PTZC** shows higher V_{oc} than **BzC**.

The chemical capacitance (C_μ) at the TiO$_2$/dye/electrolyte interface is also a useful parameter which can also give information about E_{CB}, a trap distribution parameter denoted as α (the exponential shape of TiO$_2$ in Figure 7) and the number of trap states denoted as N_t. Equation (7)[44] expresses the exponential relationship between C_μ and voltage together with the dependency of C_μ on parameters listed above.

$$C_\mu = L(1-p)\alpha \frac{q^2 N_t}{k_B T} \exp\left[\frac{\alpha(E_{redox}-E_{CB})}{k_B T}\right]\exp\left[\frac{\alpha q V}{k_B T}\right]C_\mu = C_0 \exp\left[\frac{\alpha q V}{k_B T}\right] \quad (7)$$

As seen from the equivalent circuit in Figure S5, Supporting Information, constant phase element (CPE) was used for fitting instead of capacitor. CPE was converted to the equivalent

capacitance, hereafter C_μ, using Equation (8).[38]

$$C_\mu = \frac{(R\,Q)^{\frac{1}{w}}}{R} \quad (8)$$

where R is the resistor parallel to the corresponding CPE, Q is the CPE prefactor, and w is the CPE index. The linear fitting to Equation (7) allows α to be extracted, giving 0.42 and 0.36 for **BzC** and **PTZC**, respectively. Figure 8B exhibits that **BzC** has lower C_μ than **PTZC** at the same voltage. From Equation (7), it suggests that the lower C_μ in **BzC** may originate from lower N_t at the same voltage with similar α. To show the trend in C_μ quantitatively from **BzC** and **PTZC**, N_t was estimated by Equation (7) together with the corresponding $E_{CB}-E_{F,redox}$ (from R_t results in Table 4) and α (from linear fitting to Equation (7)) through the intercepts of $\ln(C_\mu)$ versus V (Figure 8B). The results of estimated N_t are tabulated in Table 4. It is clearly seen that **PTZC** device possesses ≈9 times larger N_t than **BzC**. As suggested in Equation (7) that C_μ is proportional to N_t, the consequence of lower N_t results in lower C_μ in **BzC** at the same voltage. Thus, from the results of C_μ and R_t, they suggest that **BzC** and **PTZC** modify the trap states differently, and **PTZC** shows more upward displacement in E_{CB}.

EIS results also allow the recombination resistance (R_{rec}) at the TiO$_2$/dye/electrolyte interface to be determined. The dependency of R_{rec} on voltage can be expressed in Equation (9)[44]

$$R_{rec} = \frac{\sqrt{\pi\lambda k_B T}}{q^2 L\alpha k_r c_{ox} N_s}\exp\left[\alpha\left(\frac{E_{CB}-E_{F,redox}}{k_B T}\right)-\frac{\lambda}{4k_B T}\right]\exp\left[-\frac{qV}{mk_B T}\right]$$

$$R_{rec} = R_0 \exp\left[-\frac{qV}{mk_B T}\right] \quad (9)$$

where λ is reorganization energy of acceptor species in the electrolyte, c_{ox} is the concentration of acceptor species in the electrolyte, k_r denotes the rate constant for recombination kinetics, N_s is the total number of surface states contributing to interfacial
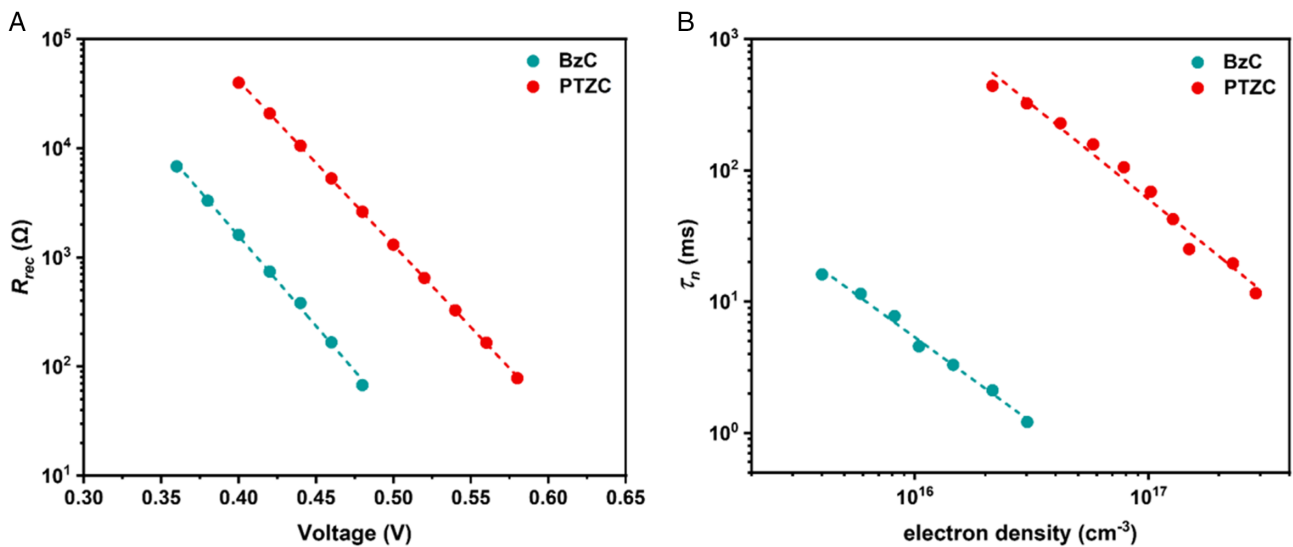

Figure 9. A) Recombination resistance (R_{rec}) as a function of voltage where dotted lines show the fitting according to Equation (9) and B) electron lifetime (τ_n) as a function of electron density (n).

recombination, and m denotes ideality factor explaining the coefficient determining nonlinear charge transfer. Fitting R_{rec} against voltage exhibits an exponential decrease in R_{rec} with increasing voltage, as shown **Figure 9**A. The results show that **PTZC** exhibits larger R_{rec} than **BzC**, which implies more efficient charge recombination retardation from **PTZC**. Furthermore, this fitting enables m to be determined and the results are shown in Table 4. Normally, the value of m for DSSCs is larger than 1 due to nonlinear charge transfer through surface trap states.[40] Therefore, the relatively low values of m (close to 1) from **BzC** and **PTZC** may suggest efficient suppression of electron recombination from surface trap states with higher degree of the suppression from **BzC**. Recently, Zhang et al. reported a low value of m (1.08) obtained by dye **MS5**.[45] As shown in Table 4, **PTZC** shows m value of 1.12 which is close to the above value reported. Moreover, **BzC** achieved even lower m (1.03), which is the lowest value reported.

To gain further insight into recombination kinetics between **BzC** and **PTZC**, electron lifetime (τ_n) was calculated by Equation (10).[46]

$$\tau_n = C_\mu R_{rec} \tag{10}$$

As highlighted by Barnes et al., charge concentration can be used to decouple the contribution of voltage to differences in electron recombination observed between devices.[41] Therefore, total electron density (n) should be used as a basis to compare the electron recombination instead of voltage. The total electron density (n) can be determined by Equation (11)[41]

$$n = \frac{C_\mu k_B T}{q^2 L \alpha} \tag{11}$$

Figure 9B illustrates τ_n as a function of n in which both dyes show exponential decrease in τ_n with increasing n. It is clearly seen that **PTZC** has much longer electron lifetime than **BzC** at the same electron density. This indicates that the recombination kinetics of electron with acceptor species in electrolyte is much slower for **PTZC** than **BzC**. Thus, the longer electron lifetime for **PTZC** enables higher V_{oc}, which is consistent with J–V curve results (Table 3).

Overall, the EIS results reveal the different influence of each dye to the energetics and kinetics of the device. Changing from **BzC** to **PTZC** gives rise to both an upward shift in E_{CB}, and also slower electron recombination kinetics under the same total electron density, which prolongs electron lifetime. These points together explain the higher V_{oc} for the device sensitized with **PTZC** than that sensitized with **BzC**. Moreover, analysis of R_{rec} results reveal that both dyes effectively suppress interfacial charge recombination from surface states as seen by relatively low m values.

To rationalize these effects in terms of dye properties, the effect of dye structure on E_{CB} is discussed below. The energetics of TiO$_2$ can be explained in terms of dipole moment of dyes and dye coverage, as suggested in Equation (12)[47]

$$\Delta E_{CB} = -\frac{q \vec{\mu}_{normal} \gamma}{\varepsilon_0 \varepsilon} \tag{12}$$

where ΔE_{CB} is the shift in TiO$_2$ CB, γ is the dye surface concentration, $\vec{\mu}_{normal}$ is the dipole moment component of individual

molecule perpendicular to TiO$_2$ surface, and ε_0 and ε are the dielectric constant of the monolayer and the permittivity of the vacuum, respectively. Equation (12) suggests that higher dye surface concentration and larger $\vec{\mu}_{normal}$ cause the negative shift (upward shift) in E_{CB}. The total dipole moment (μ_{total}) is used to compare the effect of dipole moment on E_{CB} shift by assuming that the orientation of the dye is perpendicular to TiO$_2$ surface. From DFT calculations results, the dipole moments of **BzC** and **PTZC** are 11.08 and 12.07 D, respectively (**Figure 10**). Although μ_{total} of **BzC** and **PTZC** are similar, the angle of μ_{total} with respect to $\vec{\mu}_{normal}$ for **BzC** is larger than that of **PTZC**. It suggests that μ_{total} of **PTZC** induces more upward shift in E_{CB}, compared with **BzC**, as the direction of μ_{total} of **PTZC** is more perpendicular to TiO$_2$ surface or closer to $\vec{\mu}_{normal}$.[48] Moreover, the dye uptake results (Table 3) show that **PTZC** exhibits higher dye-loading amount than **BzC**, implying better dye coverage (relating to γ) from **PTZC**. Thus, the combined results between the dipole moment and dye coverage indicate the trend in more upward shift in E_{CB} from **PTZC**. Apart from the shift in E_{CB}, **PTZC** structure is composed of PTZ unit featuring the hexyl chain. It is well known that the long alkyl chain can retard electron recombination with acceptor species in the electrolyte.[49,50] This may also contribute to slower recombination kinetics for **PTZC**.

2.6. Synthesis Cost Analysis

Most reported DSSC dyes were synthesized using versatile Pd cross-coupling reactions. In such studies, the amount of Pd catalyst may not be optimized and the typical %loading range may fall around 5–10%. This may be more than the reaction needs, leading to higher synthesis costs. Although efforts to optimize the %loading of Pd catalysts could make some contribution to lower costs, using alternative Pd-free reactions circumvents the issue entirely. Hence, in our case, we have used the HWE reaction to connect the donor and π-spacer. To demonstrate the concept of alternative reactions for Pd cross-coupling reactions and low-cost donor moiety, the synthesis costs of **BzC** and **PTZC** are calculated. This estimation is only based on the preparation cost in which the work-up and purification costs are not included as they depend on the
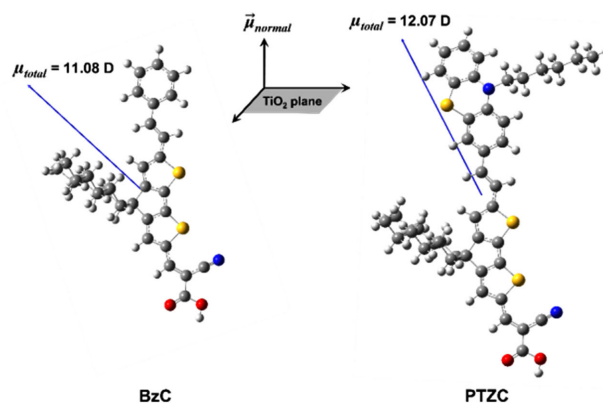

Figure 10. The total dipole moments of **BzC** and **PTZC** calculated by DFT calculations in DCM solvation model together with $\vec{\mu}_{normal}$ direction that is perpendicular to TiO$_2$ surface.

ADVANCED
SCIENCE NEWS
www.advancedsciencenews.com

Solar
RRL
www.solar-rrl.com

scale of the synthesis and the purification techniques may be substituted by other appropriate techniques for the larger-scale synthesis. The estimated cost analysis was carried out following Maciejczyk et al.,[51] which is based on 1 gram of product. The synthesis yield at each step was taken into account in the cost estimation (Scheme 1 and 2). Table S1 and S2, Supporting Information, depict the estimated synthesis cost for the CPDT unit from two-step reactions. The overall cost for the CPDT unit for the next steps is $37.43 g^{-1}. The synthesis of **BzC** comprises four steps and the corresponding cost analysis for each step is shown in Table S3–S6, Supporting Information. The total estimated synthesis cost for **BzC** is $50.06 g^{-1}. In the case of **PTZC**, there are 7 steps involved in the synthesis and the corresponding cost analysis for each step is depicted in Table S7–S13, Supporting Information. The total estimated synthesis cost for **PTZC** is $61.94 g^{-1}. From the estimation, one can see that the large share of the synthesis cost is the CPDT unit, accounting for ≈63% of the total synthesis cost.

To prove the concept of the cost-effective synthesis, **LEG-4**, one of the efficient commercial dyes, was chosen to compare with **BzC** and **PTZC** (see the synthetic method and structure in Scheme S1, Supporting Information). Unless stated otherwise, the synthesis methods and yields were taken from Gabrielsson et al.[11] and only material costs are considered so as to allow the direct comparison with **BzC** and **PTZC**. Table S14–S22, Supporting Information, show 10 steps of **LEG-4** synthesis, including relevant intermediates, and the estimated synthesis cost of **LEG-4**. The total synthesis cost of **LEG-4** is estimated to be $467.63 g^{-1}. It is clearly seen that approximately 65% ($310) of the total synthesis cost falls in the synthesis of the donor part as it involves an expensive boronic acid derivative. Moreover, the prices of the Pd catalysts for the Suziki–Miyaura crosscoupling used to synthesize **LEG-4** are more than or equal to the total synthesis price of **BzC** and **PTZC**, respectively. When compared with **BzC** and **PTZC**, the total synthesis cost of **LEG-4** is around 7.5-9 times higher than those for **BzC** and **PTZC**. This indicates the possibility of alternative Pd-free reactions for dye synthesis. For example, in our case, we show that the HWE reaction to link the donor with π-spacer is endowed with the potential for cost-effective synthesis which may be able to replace Pd cross-coupling reaction. It is also worth highlighting the use of hazardous pyrophoric reagents, such as *n*-BuLi, when considering large-scale synthesis. Although the synthesis of CPDT may need *n*-BuLi as one of the reagents, we have avoided the use of pyrophoric reagents in subsequent steps (Scheme 2), and this can also serve as a guide toward more sustainable dye design and synthesis in the future.

Finally, for a complete picture of the cost analysis, the photovoltaic performance needs to be taken into account to determine the cost performance. Note that the associated cost of glass, TiO_2, Pt, and electrolyte is not taken into account. The DSSC devices with **LEG-4** were also fabricated with I^-/I_3^- electrolyte to reference the cost performance. The photovoltaic results show that the best device (from three individual cells) with **LEG-4** attained PCE of 7.41% (Table 3), which compares favorably well with literature.[52] The cost performance calculation was determined by cost per unit area per %PCE following Tanaka et al.[53] The calculated results are shown in **Table 5**. Although the synthesis cost of **BzC** is lower than that of **PTZC**, the cost performance of **PTZC** is only 3.12% higher than that of **BzC** when considering the photovoltaic

Table 5. The estimated cost performance of **BzC**, **PTZC**, and **LEG-4**.

Dye	Cost [$ g^{-1}]	Quantity [mol cm^{-2}][a]	Cost [$ cm^{-2}]	Cost performance [$ cm^{-2}/%PCE]
BzC	50.06	1.78×10^{-7}	0.0048	0.160
PTZC	61.94	2.11×10^{-7}	0.0098	0.165
LEG-4	467.63	1.22×10^{-7}	0.0640	0.867

[a]The values were estimated from dye desorption (Table 3).

performance. This is due to higher photovoltaic performance obtained from **PTZC** and comparable synthesis cost of **PTZC** with **BzC**. When compared with **LEG-4**, it is clearly seen that the cost performance of **BzC** and **PTZC** are around 5 times cheaper than that of **LEG-4**. This is due to the much lower synthesis cost and broadly comparable PCE (5.92% for **PTZC** and 7.41% for **LEG-4**). The cost performances of **PTZC** could be even lower if meticulous device optimizations were carried out.

3. Conclusion

Two new dyes (**BzC** and **PTZC**) based on low-cost donor moiety and simple structures were successfully synthesized with Pd-free reactions. The aims of Pd-free synthesis are not only to reduce the synthesis cost but also to highlight environmental concerns, especially when the Stille crosscoupling is used in the synthesis. For optical properties, both dyes exhibit high extinction coefficient with **PTZC** showing slightly higher extinction coefficient compared with **BzC**. Due to large conjugation in **PTZC**, it shows the first oxidation potential of about 0.35 V less than that of **BzC**. The study on photovoltaic performance reveals that **PTZC** shows better efficiency with around 6% obtained from the best device. The higher J_{sc} for **PTZC** is attributed to better light harvesting efficiency and more dye loading on the TiO_2 film. The EIS measurements reveal that **BzC** and **PTZC** exhibit relatively low ideality factor (m) with the values of 1.03 and 1.12, respectively, indicating efficient suppression of electron recombination from surface trap states. The device with **PTZC** shows slower recombination kinetics and upward shift of TiO_2 conduction band, leading to higher V_{oc} than **BzC**. We also demonstrated the cost analysis for the synthesis of **BzC** and **PTZC**, which are estimated to be around $50 g^{-1} and $60 g^{-1}, respectively. When compared to **LEG-4** used as the reference dye, the synthesis costs of **BzC** and **PTZC** are around 7.5-9 times lower. Moreover, the overall yields of **BzC** and **PTZC** are very high (around 55–70%) which can be scalable. The comparison of the **BzC** and **PTZC** cost performances with **LEG-4** reveals that they are around 20% of the cost of **LEG-4** per cm^2 per %PCE. Indeed, the efficiency does matter but we also believe that when it comes to practical use, that is, large-scale production, the associated price should be taken into account.

4. Experimental Section

Dye Synthesis: All reagents were purchased from Sigma-Aldrich (Merck), Alfa-Aesar, Fisher Scientific, Acros Organics, and Fluorochem unless stated otherwise and were used without further purification. CPDT was purchased from Shanghai Qinghang Chemical Co. Ltd.,

China, and was used as received. The synthetic methodology of **BzC** and **PTZC** is described as follows.

Synthesis of 4,4-Dihexyl-4 H-Cyclopenta[2,1-b:3,4-b']dithiophene (1): CPDT (1.50 g, 8.42 mmol), 1-bromohexane (3.6 mL, 25.7 mmol), and KI (0.14 g, 0.84 mmol) were dissolved in 60 mL of DMSO and bubbled with N_2 for 10 min. Ground KOH (1.92 g, 34.2 mmol) was added into the mixture, and the resulting mixture was stirred overnight at room temperature in the dark. After adding distilled water, the mixture was extracted with hexane. The organic phase was collected, dried over anh. Na_2SO_4, filtered, and evaporated to remove hexane. The residue was purified by column chromatography on SiO_2 gel column eluted with hexane to obtain light yellow oil (2.67 g, 91.6%) ^{1}H NMR (500 MHz, Chloroform-d) δ 7.17 (d, J = 4.8 Hz, 2H), 6.95 (d, J = 4.9 Hz, 2H), 1.87–1.83 (m, 4H), 1.21 (dddd, J = 9.6, 7.5, 5.3, 3.7 Hz, 4H), 1.15 (ddd, J = 7.6, 4.6, 2.7 Hz, 8H), 0.97 (ddt, J = 10.1, 7.9, 5.0 Hz, 4H), 0.84 (t, J = 7.1 Hz, 6H). ^{13}C NMR (126 MHz, Chloroform-d) δ 158.15, 136.45, 124.41, 121.65, 53.26, 37.76, 31.62, 29.70, 24.49, 22.60, 14.03.

Synthesis of 4,4-Dihexyl-4 H-Cyclopenta[2,1-b:3,4-b']dithiophene-2-Carbaldehyde (2): Compound **1** (0.26 g, 0.75 mmol) was dissolved in 5 mL anh. 1,2-dichloroethane. The solution was cooled to 0 °C with an ice bath. To the solution, 0.1 mL (1.29 mmol) of anh. DMF was added and the mixture was stirred at the same temperature under N_2. Then, 0.11 mL (1.18 mmol) of $POCl_3$ was added to the cooled mixture dropwise, and the resulting mixture was stirred at the same temperature for 4 h (TLC monitor). To the completed reaction was added saturated aqueous solution of NaOAc resulting in a separation into two phases. The mixture was stirred at 50 °C for about 1.5 to 2 h. After that, the mixture was extracted with EtOAc, dried over $MgSO_4$, filtered, and evaporated to remove EtOAc. The pure product was purified by silica plug eluted with 1:1 v/v of hexane: DCM to obtain yellow oil (0.26 g, 94.7%). ^{1}H NMR (500 MHz, Chloroform-d) δ 9.83 (s, 1H), 7.57 (s, 1H), 7.40 (d, J = 4.9 Hz, 1H), 6.98 (d, J = 4.9 Hz, 1H), 1.91–1.82 (m, 4H), 1.20–1.11 (m, 12H), 0.97–0.89 (m, 4H), 0.81 (t, J = 7.0 Hz, 6H). ^{13}C NMR (126 MHz, Chloroform-d) δ 182.77, 162.60, 158.28, 147.89, 143.30, 135.72, 129.73, 121.99, 53.92, 37.79, 31.70, 29.85, 29.73, 24.68, 22.71, 14.14.

Synthesis of Diethyl Benzylphosphonate (3): Benzyl bromide (1.00 g, 5.85 mmol) and triethylphosphite (5 mL, 29.2 mmol) were added to a reaction flask. The mixture was refluxed at 135 °C for 6 h. The excess triethylphosphite was removed by distillation under vacuum to obtain pale yellow liquid (1.34 g, quant.). ^{1}H NMR (400 MHz, Chloroform-d) δ 7.35–7.27 (m, 5H), 4.03 (dqd, J = 8.2, 7.1, 3.2 Hz, 4H), 3.18 (d, J = 21.6 Hz, 2H), 1.26 (t, J = 7.1 Hz, 6H).

Synthesis of (E)-4,4-Dihexyl-2-Styryl-4 H-Cyclopenta[2,1-b:3,4-b']Dithio-Phene (4): Compound **3** (0.28 g, 1.23 mmol) and compound **2** (0.29 g, 0.78 mmol) were added to a reaction flask and dissolved in 5 mL of anh. THF. The mixture was cooled down to 0 °C and stirred under N_2. In another container, potassium *tert*-butoxide (KO^{t}Bu) (0.29 g, 2.58 mmol) was dissolved in 10 mL of anh. THF. The KO^{t}Bu solution was added to the cooled mixture drop wise, stirred at 0 °C, and gradually warmed up to 25 °C before being left to stir overnight under N_2. After which time, water was added to the mixture before it was extracted with EtOAc and dried over $MgSO_4$, filtered, and evaporated to remove EtOAc. The crude product was purified by column chromatography SiO_2 eluted with gradient elution of a mixture of hexane and DCM (20% increment of DCM to 80%DCM) to obtain yellow oil (0.32 g, 91.4%). ^{1}H NMR (500 MHz, Chloroform-d) δ 7.47–7.44 (m, 2H), 7.34 (t, J = 7.7 Hz, 2H), 7.25–7.17 (m, 3H), 6.93 (d, J = 4.9 Hz, 2H), 6.88 (d, J = 16.0 Hz, 1H), 1.85–1.79 (m, 4H), 1.22–1.12 (m, 12H), 1.04–0.92 (m, 4H), 0.82 (t, J = 7.0 Hz, 6H). ^{13}C NMR (126 MHz, Chloroform-d) δ 158.55, 158.53, 143.20, 137.43, 128.85, 127.39, 126.25, 126.19, 125.28, 123.03, 121.78, 121.08, 53.70, 37.92, 31.78, 29.86, 24.66, 22.77, 14.18. MS (ESI): [M + H]$^+$ Calcd for $C_{29}H_{36}S_2$: 449.2331; found: 449.2330.

Synthesis of (E)-4,4-Dihexyl-6-Styryl-4 H-Cyclopenta[2,1-b:3,4-b']dithiophene-2-Carbaldehyde (5): Compound **4** (0.31 g, 0.69 mmol) was dissolved in 5 mL anh. 1,2-dichloroethane, and the solution was cooled down to 0 °C with an ice bath. To the solution, 0.17 mL (2.19 mmol) of anh. DMF was added and the mixture was stirred at the same temperature under N_2. Then, 0.10 mL (1.07 mmol) of $POCl_3$ was added to the cooled mixture

drop wise, and the resulting mixture was stirred at the same temperature for 4 h (TLC monitor). To the completed reaction was added saturated aqueous solution of NaOAc resulting in a separation into two phases. The mixture was stirred at 50 °C for about 1.5 to 2 h. After that, the mixture was extracted with EtOAc, dried over $MgSO_4$, filtered, and evaporated to remove EtOAc. The pure product was purified by silica plug eluted with a mixture of hexane and DCM with 20% increment of DCM to 80%DCM to obtain orange wax (0.32 g, 95.8%). ^{1}H NMR (500 MHz, Methylene Chloride-d$_2$) δ 9.82 (d, J = 2.1 Hz, 1H), 7.58 (d, J = 2.0 Hz, 1H), 7.50 (dd, J = 7.3, 2.0 Hz, 2H), 7.37 (td, J = 7.8, 2.0 Hz, 2H), 7.31–7.24 (m, 2H), 7.04–6.99 (m, 2H), 1.94–1.86 (m, 4H), 1.21–1.14 (m, 12H), 0.96 (p, J = 7.8 Hz, 4H), 0.82 (td, J = 7.0, 2.1 Hz, 6H). ^{13}C NMR (126 MHz, Methylene Chloride-d$_2$) δ 182.94, 163.54, 158.84, 148.43, 144.08, 137.33, 135.14, 130.61, 129.38, 128.93, 128.47, 126.94, 122.78, 121.42, 54.69, 38.20, 32.15, 30.26, 30.17, 25.09, 23.14, 14.34. MS (ESI): [M + H]$^+$ Calcd for $C_{30}H_{36}OS_2$: 477.2280; found: 477.2282.

Synthesis of (E)-2-Cyano-3-(4,4-Dihexyl-6-((E)-Styryl)-4 H-Cyclopenta-[2,1-b:3,4-b']-Dithiophen-2-yl)acrylic Acid (BzC): 0.18 × g (2.12 mmol) of cyanoacetic acid was added in a reaction flask equipped with a condenser. Compound **5** (0.25 g, 0.53 mmol) was dissolved in 10 mL of anh. $CHCl_3$ and transferred to the reaction flask. The mixture was stirred at 75 °C for about 2 min before adding 0.42 mL (4.24 mmol) of piperidine. The resulting mixture was refluxed at 75 °C for 6 h (TLC monitor). After that, the mixture was diluted with DCM and extracted with 1 M HCl and the DCM phase was collected, dried over Na_2SO_4, filtered, and evaporated to remove DCM. The crude product was purified by dry column vacuum chromatography (DCVC) technique with gradient elution (hexane to DCM with 10% increment of DCM, pure DCM for 10 fractions, and DCM to 20% MeOH with 2% increment of MeOH). The pure product was diluted with DCM, extracted with 1 M HCl, dried over $MgSO_4$, filtered, and evaporated to obtain pink solid (0.26 g, 90.2%). ^{1}H NMR (500 MHz, Methylene Chloride-d$_2$) δ 8.34 (s, 1H), 7.63 (s, 1H), 7.54–7.48 (m, 2H), 7.38 (t, J = 7.7 Hz, 2H), 7.31–7.26 (m, 2H), 7.05 (d, J = 16.4 Hz, 2H), 1.91 (dp, J = 10.0, 6.8 Hz, 4H), 1.22–1.13 (m, 12H), 0.96 (p, J = 7.4 Hz, 4H), 0.82 (t, J = 7.0 Hz, 6H). ^{13}C NMR (126 MHz, Methylene Chloride-d$_2$) δ 164.36, 158.96, 150.92, 149.79, 148.07, 136.58, 136.33, 134.56, 129.22, 128.82, 128.11, 126.48, 122.05, 120.87, 116.80, 54.15, 37.64, 31.55, 29.54, 24.51, 22.55, 13.75. MS (ESI): [M + H]$^+$ Calcd for $C_{33}H_{37}NO_2S_2$: 544.2338; found: 544.2334. Anal. Calcd for $C_{33}H_{37}NO_2S_2$: C, 72.89%; H, 6.86%; N, 2.58%; found: C, 72.53%; H, 7.12%; N, 2.13%.

Synthesis of 10-Hexyl-10 H-Phenothiazine (6): Phenothiazine (PTZ) (3.00 g, 15.05 mmol), 1-bromohexane (3.2 mL, 22.87 mmol), and KI (0.4 g, 2.41 mmol) were dissolved in 50 mL of DMSO and bubbled with N_2 for 10 min. Ground KOH (2.60 g, 46.3 mmol) was added into the mixture, and the resulting mixture was stirred overnight at room temperature in the dark. After adding distilled water, the mixture was extracted with ether. The organic phase was collected, dried over anh. $MgSO_4$, filtered, and evaporated to remove ether. The residue was purified by column chromatography on SiO_2 gel eluted with 2% EtOAc in hexane to obtain pale yellow oil (4.05 g, 95.0%). ^{1}H NMR (500 MHz, Methylene Chloride-d$_2$) δ 7.15 (ddd, J = 8.2, 7.4, 1.6 Hz, 2H), 7.11 (dd, J = 7.6, 1.5 Hz, 2H), 6.91 (dd, J = 7.5, 1.2 Hz, 2H), 6.90–6.87 (m, 2H), 3.86–3.82 (m, 2H), 1.82–1.74 (m, 2H), 1.47–1.39 (m, 2 H), 1.30 (h, J = 3.6 Hz, 4H), 0.89–0.86 (m, 3H). ^{13}C NMR (126 MHz, Methylene Chloride-d$_2$) δ 145.96, 127.79, 127.77, 122.82, 125.34, 116.03, 47.93, 32.04, 27.42, 27.16, 23.18, 14.32.

Synthesis of 10-Hexyl-10 H-Phenothiazine-3-Carbaldehyde (7): Compound **6** (0.46 g, 1.62 mmol) was diluted in 10 mL of anh. 1,2-dichloroethane in a reaction flask equipped with a condenser and the solution was cooled down to 0 °C. In another container, 0.45 mL (4.83 mmol) of $POCl_3$ was added dropwise to a cooled solution of anh. DMF (0.63 mL, 8.14 mmol) in 5 mL of anh. 1,2-dichloroethane. The mixture of $POCl_3$ and DMF was added to the solution of compound **6** dropwise while being stirred at 0 °C. After that, the mixture was refluxed at 90 °C for 4 h. To the mixture was added saturated aqueous solution of NaOAc and stirred at 50 °C for 1 h. Then, the mixture was extracted with EtOAc, dried over $MgSO_4$, filtered, and evaporated to remove EtOAc. The crude product was purified by column chromatography on SiO_2 and eluted with 15%

EtOAC:85%hexane to obtain yellow solid (0.40 g, 80.0%). ^{1}H NMR (500 MHz, Methylene Chloride-d_2) δ 9.78 (s, 1H), 7.63 (dd, $J = 8.4$, 2.0 Hz, 1H), 7.56 (d, $J = 2.0$ Hz, 1H), 7.18 (ddd, $J = 8.1$, 7.3, 1.6 Hz, 1H), 7.11 (dd, $J = 7.6$, 1.6 Hz, 1H), 6.99–6.90 (m, 3H), 3.92–3.88 (m, 2H), 1.83–1.77 (m, 2H), 1.48–1.41 (m, 2H), 1.33–1.29 (m, 4H), 0.90 – 0.85 (m, 3H). ^{13}C NMR (126 MHz, Methylene Chloride-d_2) δ 190.19, 151.13, 143.98, 131.58, 130.48, 128.32, 127.98, 127.79, 125.33, 124.12, 123.87, 116.48, 115.31, 60.64, 48.40, 31.79, 27.09, 26.86, 22.99, 21.19, 14.41, 14.13.

Synthesis of (10-Hexyl-10 H-Phenothiazin-3-yl)methanol (8): Compound **7** (0.40 g, 1.28 mmol) was dissolved in 12 mL of THF:MeOH (5:1 v v^{-1}) mixture. After that, NaBH$_4$ (0.1 g, 2.64 mmol) was added to the solution portion wise, and bubbles formed upon adding NaBH$_4$. The mixture was stirred at room temperature for 1.5 h during which time, the colour of solution changed from bright yellow to pale yellow. After that, the mixture was evaporated and redissolved in EtOAc, followed by extraction with brine, dried over MgSO$_4$, filtered, and evaporation. The crude product was purified by silica plug with 70%hexane:30%EtOAc elution to obtain pale yellow oil (0.40 g, quant.). ^{1}H NMR (500 MHz, Methylene Chloride-d_2) δ 7.17–7.12 (m, 2H), 7.11 (dd, $J = 7.7$, 1.7 Hz, 2H), 6.91 (dd, $J = 7.5$, 1.2 Hz, 1H), 6.89–6.86 (m, 1H), 6.85 (d, $J = 8.2$ Hz, 1H), 4.54 (d, $J = 5.7$ Hz, 2H), 3.86–3.81 (m, 2H), 1.80–1.74 (m, 2H), 1.64 (t, $J = 5.9$ Hz, 1H), 1.45–1.41 (m, 2H), 1.32–1.28 (m, 4H), 0.89 – 0.85 (m, 3H). ^{13}C NMR (126 MHz, CD$_2$Cl$_2$) δ 145.71, 145.11, 135.80, 127.66, 127.64, 126.53, 126.46, 125.31, 124.91, 122.67, 115.82, 115.74, 64.80, 47.82, 31.87, 27.22, 26.98, 23.01, 14.15. MS (ESI): [M−H]$^-$ Calcd for C$_{19}$H$_{22}$NOS: 312.1417; found: 312.1419.

Synthesis of Diethyl ((10-Hexyl-10 H-Phenothiazin-3-yl)methyl)-Phosphonate (9): In an oven-dried flask equipped with a condenser, ZnI$_2$ (0.32 g, 1.00 mmol) was added, followed by evacuation, and refilled with N$_2$ for three times. The solid ZnI$_2$ was suspended in 5 mL anh. THF before adding 0.22 mL (1.28 mmol) of triethylphosphite. In another container, compound **8** (0.20 g, 0.65 mmol) was dissolved in 10 mL of anh. THF. After that, the solution of compound **8** was added in the above mixture of ZnI$_2$ and triethylphosphite, followed by reflux at 75 °C for 16 h. The mixture was diluted with ether and extracted with 2 M NaOH. The ether phase was collected, dried over MgSO$_4$, filtered, and evaporated. The crude product was distilled under vacuum to remove excess triethylphosphite to obtain light yellow oil (0.25 g, 90.0%). ^{1}H NMR (500 MHz, Methylene Chloride-d_2) δ 7.15 (ddd, $J = 7.6$, 5.2, 2.7 Hz, 1H), 7.12–7.09 (m, 1H), 7.06 (dq, $J = 7.3$, 2.4 Hz, 1H), 7.03 (q, $J = 2.6$ Hz, 1H), 6.92–6.85 (m, 2H), 6.83–6.80 (m, 1H), 4.04–3.96 (m, 4H), 3.82 (t, $J = 7.2$ Hz, 2H), 3.04 – 2.97 (m, 2H), 1.81–1.74 (m, 2H), 1.45–1.40 (m, 2H), 1.31 (dt, $J = 7.1$, 3.5 Hz, 4H), 1.25 (td, $J = 7.2$, 3.4 Hz, 6H), 0.87 (td, $J = 6.2$, 3.4 Hz, 3H). ^{13}C NMR (126 MHz, Methylene Chloride-d_2) δ 145.69, 144.51, 128.96, 128.65, 127.63, 126.25, 125.22, 124.79, 122.61, 115.76, 115.68, 62.42, 47.78, 33.39, 32.29, 31.87, 30.10, 27.17, 26.98, 16.63, 14.15. ^{31}P NMR (202 MHz, Methylene Chloride-d_2) δ 25.97. MS (ESI): [M + H]$^+$ Calcd for C$_{23}$H$_{33}$NO$_3$SP: 434.1913; found: 434.1920.

Synthesis of (E)-3-(2-(4,4-Dihexyl-4 H-Cyclopenta[2,1-b:3,4-b′]dithiophen-2-yl)vinyl)-10-Hexyl-10 H-Phenothiazine (10): Compound **9** (0.58 g, 1.34 mmol) and compound **2** (0.42 g, 1.12 mmol) were dissolved in 10 mL of anh. THF and the solution was cooled down to 0 °C. In another container, KO^{t}Bu (0.31 g, 2.75 mmol) was dissolved in 10 mL of anh. THF. The KO^{t}Bu solution was added to the cooled mixture dropwise, stirred at 0 °C, and gradually warmed up to 25 0 °C before being left to stir overnight under N$_2$. After this, water was added to the mixture before it was extracted with DCM and dried over MgSO$_4$, filtered, and evaporated to remove DCM. The crude product was purified by column chromatography SiO$_2$ with 20%DCM:80%hexane elution to obtain yellow wax (0.70 g, 95.6%). ^{1}H NMR (500 MHz, Methylene Chloride-d_2) δ 7.27 (h, $J = 2.1$ Hz, 2H), 7.23 (d, $J = 4.8$ Hz, 1H), 7.20 (ddd, $J = 8.1$, 7.3, 1.6 Hz, 1H), 7.17–7.12 (m, 2H), 6.99 (d, $J = 4.8$ Hz, 1H), 6.97–6.93 (m, 2H), 6.92 (dd, $J = 8.1$, 1.2 Hz, 1H), 6.88 (d, $J = 9.0$ Hz, 1H), 6.81 (d, $J = 16.0$ Hz, 1H), 3.91–3.87 (m, 2H), 1.92–1.80 (m, 6H), 1.48 (t, $J = 7.7$ Hz, 2H), 1.38–1.33 (m, 4H), 1.29–1.13 (m, 12H), 1.06–0.94 (m, 4H), 0.94–0.90 (m, 3H), 0.85 (t, $J = 7.0$ Hz, 6H). ^{13}C NMR (126 MHz, Methylene Chloride-d_2)

δ 159.00, 158.88, 145.34, 144.82, 143.69, 136.96, 135.84, 132.13, 127.67, 125.86, 125.46, 125.35, 125.16, 124.69, 124.51, 122.75, 122.13, 121.58, 121.07, 115.83, 47.93, 38.16, 32.05, 31.88, 30.10, 27.23, 26.98, 24.91, 23.02, 14.18. MS (ESI): [M]$^+$ Calcd for C$_{41}$H$_{51}$NS$_3$: 653.3178; found: 653.3165.

Synthesis of (E)-4,4-Dihexyl-6-(2-(10-Hexyl-10 H-Phenothiazin-3-yl)vinyl)-4 H-Cyclo-Penta[2,1-b:3,4-b′]dithiophene-2-Carbaldehyde (11): Compound **10** (0.30 g, 0.46 mmol) was dissolved in 5 mL anh. 1,2-dichloroethane and the solution was cooled down to 0 °C with an ice bath. To the solution, 0.11 mL (1.42 mmol) of anh. DMF was added and the mixture was stirred at the same temperature under N$_2$. Then, 0.10 mL (1.07 mmol) of POCl$_3$ was added to the cooled mixture dropwise, and the resulting mixture was stirred at the same temperature for 4 h (TLC monitor). To the completed reaction was added saturated aqueous solution of NaOAc resulting in a separation into two phases. The mixture was stirred at 50 °C for about 1.5 to 2 h. After that, the mixture was extracted with EtOAc, dried over MgSO$_4$, filtered, and evaporated to remove EtOAc. The pure product was purified by silica plug eluted with gradient elution of a mixture of hexane and DCM (20% increment of DCM to 80%DCM) to obtain red wax (0.29 g, 95.0%). ^{1}H NMR (500 MHz, Methylene Chloride-d_2) δ 9.81 (s, 1H), 7.57 (s, 1H), 7.26 (h, $J = 2.3$ Hz, 2H), 7.16 (ddd, $J = 8.1$, 7.4, 1.6 Hz, 1H), 7.14–7.09 (m, 2H), 6.97 (s, 1H), 6.92 (td, $J = 7.5$, 1.1 Hz, 1H), 6.90 (d, $J = 1.1$ Hz, 1H), 6.89–6.84 (m, 2H), 3.89–3.81 (m, 2H), 1.95–1.76 (m, 6H), 1.48–1.42 (m, 2H), 1.32 (ddd, $J = 7.4$, 4.3, 3.0 Hz, 4H), 1.25–1.09 (m, 12H), 0.95 (p, $J = 7.7$ Hz, 4H), 0.91–0.86 (m, 3H), 0.81 (t, $J = 7.0$ Hz, 6H). ^{13}C NMR (126 MHz, Methylene Chloride-d_2) δ 182.70, 163.50, 158.52, 148.66, 147.82, 145.39, 145.18, 143.73, 134.54, 131.55, 130.42, 127.75, 127.67, 126.32, 125.43, 124.97, 124.40, 122.89, 120.90, 120.73, 115.90, 115.85, 54.49, 47.97, 38.05, 31.99, 31.87, 30.10, 30.01, 27.21, 26.97, 24.92, 23.02, 22.98, 14.18, 14.16. MS (ESI): [M]$^+$ Calcd for C$_{45}$H$_{51}$NOS$_3$: 681.3127; found: 681.3111.

Synthesis of (E)-2-Cyano-3-(4,4-Dihexyl-6-((E)-2-(10-Hexyl-10 H-Phenothiazin-3-yl)vinyl)-4 H-Cyclopenta[2,1-b:3,4-b′]dithiophen-2-yl)-Acrylic Acid (PTZC): 0.16 × g (1.90 mmol) of cyanoacetic acid was added in a reaction flask equipped with a condenser. Compound **11** (0.33 g, 0.48 mmol) was dissolved in 10 mL of anh. CHCl$_3$ and transferred to the reaction flask. The mixture was stirred at 75 °C for about 2 min before adding 0.38 mL (3.85 mmol) of piperidine. The resulting mixture was refluxed at 75 °C for 6 h (TLC monitor). After that, the mixture was diluted with DCM and extracted with 1 M HCl and the DCM phase was collected, dried over Na$_2$SO$_4$, filtered, and evaporated to remove DCM. The crude product was purified by DCVC technique with gradient elution (hexane to DCM with 10% increment of DCM, pure DCM for 15 fractions and DCM to 20% MeOH with 2% increment of MeOH). The pure product was diluted with DCM, extracted with 1 M HCl, dried over MgSO$_4$, and evaporated to obtain purple solid (0.32 g, 90.4%). 1H NMR (601 MHz, Methylene Chloride-d_2) δ 8.33 (s, 1H), 7.62 (s, 1H), 7.27 (h, $J = 2.2$ Hz, 2H), 7.18 – 7.11 (m, 3H), 6.98 (s, 1H), 6.94 (d, $J = 3.4$ Hz, 1H), 6.93 – 6.91 (m, 1H), 6.89 (dd, $J = 8.3$, 1.2 Hz, 1H), 6.87 – 6.84 (m, 1H), 3.86 (t, $J = 7.3$ Hz, 2H), 1.90 (dp, $J = 10.3$, 7.2 Hz, 4H), 1.82 – 1.77 (m, 2H), 1.47 – 1.42 (m, 2H), 1.33 – 1.29 (m, 4H), 1.22 – 1.12 (m, 12H), 0.99 – 0.93 (m, 4H), 0.90 – 0.87 (m, 3H), 0.82 (t, $J = 7.1$ Hz, 6 H). ^{13}C NMR (151 MHz, Methylene Chloride-d_2) δ 167.89, 165.06, 159.29, 151.74, 150.80, 148.47, 145.61, 145.08, 136.56, 134.56, 131.36, 128.63, 127.77, 127.67, 126.55, 125.43, 125.06, 124.34, 122.94, 120.76, 120.69, 117.25, 115.92, 115.85, 92.02, 54.53, 47.99, 38.07, 31.98, 31.87, 29.97, 27.19, 26.96, 24.93, 23.00, 14.17. MS (ESI): [M + Na]$^+$ Calcd for C$_{45}$H$_{52}$N$_2$O$_2$S$_3$: 771.3083; found: 771.3076. Anal. Calcd for C$_{45}$H$_{52}$N$_2$O$_2$S$_3$: C, 72.15%; H, 7.00%; N, 3.74%; found: C, 71.68%; H, 7.24%; N, 3.40%.

Dye Structure Characterizations: ^{1}H and ^{13}C NMR spectra were recorded on Bruker Advance 400, 500 or 600 spectrometers (500/601 MHz for ^{1}H and 126/151 MHz for ^{13}C). ^{31}P NMR spectrum was recorded on Bruker Advance 500 (202 MHz for ^{31}P). All chemical shifts were reported in parts per million (ppm) and coupling constants (J) were given in hertz (Hz). The deuterated solvents used for NMR were standardized by the solvent residual signal for ^{1}H and ^{13}C. MS were recorded on ThermoElectron MAT 900 using electrospray ionization (ESI) technique. Elemental analyses were

carried out by O. McCullough at London Metropolitan University using a Carlo Erba CE1108 Elemental Analyzer.

Optical Characterization: UV−vis absorption spectra were recorded on Jasco V-670 UV/vis/NIR spectrophotometer controlled by the SpectraManager software. All solutions were prepared in DCM. All extinction coefficients were determined by the Beer-Lambert plot with various concentrations in the range of 10–35 μM of corresponding dye. The dye desorption was carried out by diluting 1 M of tetrabutylammonium hydroxide (TBAOH) in methanol to 5 mM TBAOH with DCM. The sensitised films were soaked in 5 mM TBAOH for 30 min before making up the volume with DCM. The absorption spectra were measured in a similar manner to UV–vis absorption characterization.

Electrochemical Characterization: All voltammetry measurements were performed in anhydrous DCM with 0.3 M TBAPF$_6$ as supporting electrolyte in a three-electrode system at room temperature. Each solution was purged with N$_2$ prior to measurement. The working electrode was a Pt disk while the counter electrode and reference electrode were a Pt rod and Ag/AgCl in 2 M LiCl in ethanol, respectively. All measurements were carried out using μAUTOLAB Type III potentiostat driven by the electrochemical software GPES. The scan rates used in CV were 25, 50, 100, 200, and 400 mV s^{-1}. SWV were conducted at a step potential of 2.1 mV, amplitude of 250 mV, and frequency of 25 Hz, which gave a scan rate of 52.5 mV s^{-1}. All measurements were referenced to Ferrocene/Ferrocenium (Fc/Fc$^+$) as an internal standard.

Theoretical Calculations: The molecular dye structures were built in Avogadro[54] and the drawn molecule was adjusted using basic optimization in Avogadro. The drawn molecules were optimized by using Gaussian 09[55] at B3LYP[31] level of theory with 6-31G(d) basis set under vacuum. After that, the optimized structures were subject to re-optimization in DCM (PCM solvation model).[56] The TDDFT calculations used the optimized structures in solvation model and were conducted by using Gaussian 09 at CAM-B3LYP[32] level of theory with 6-31G(d) basis set and in DCM (PCM solvation model). The 50 states of singlet electronic transitions obtained from TDDFT calculations were processed with the GaussSum software package.[57] For the dyes' dipole moment, the DFT optimized dyes in DCM solvent model were subjected to GaussView 6[58] for visualization.

Solar Cell Fabrication: Fluorine-doped tin oxide (FTO)-coated glass (Merck, 7 Ω sq^{-1}) was cleaned using 2% Hellmanex solution with sonication in deionized water for 30 min, followed by sonication in ethanol for 30 min. The cleaned glass was treated with UV–O$_3$ treatment for 20 min. After that, the cleaned and treated glass was pretreated with 40 mM aqueous solution TiCl$_4$ at 70 °C for 30 min, which was subsequently rinsed with deionized water and ethanol, respectively. The TiCl$_4$-treated glass was sintered at 500 °C for 30 min. Upon cooling down, the sintered glass was screen printed with commercial transparent TiO$_2$ paste (Ti-Nanoxide T/SP, Solaronix), followed by drying at 120 °C for 10 min. The scattering TiO$_2$ paste (Ti-Nanoxide T/SP, Solaronix) was screen printed on printed glass, followed by drying at 120 °C for 10 min. The films were annealed at 500 °C for 15 min using programmable hotplate. The resulting TiO$_2$ film thickness was 8 μm with the area of 0.28 cm^2. The sintered films were allowed to cool down and were treated with 40 mM aqueous solution TiCl$_4$ at 70 °C for 30 min, rinsed with deionized water and ethanol, and were sintered again at 500 °C for 30 min. When the temperature dropped to about 90 °C, the films were soaked in 0.5 mM dye bath containing 2.5 mM CDCA for **BzC** and **PTZC** and containing 5 mM CDCA for **LEG-4** in *tert*-butyl alcohol:acetonitrile 1:1 v/v for 20 h. The sensitised working electrodes were removed from dye bath and washed with acetonitrile to remove unadsorbed dye molecules. The counterelectrodes were predrilled on FTO glass, washed by sonicating in 0.1 M HCl in ethanol for 15 min, and followed by sonicating in ethanol for 15 min and deionized water for 15 min, respectively. The cleaned predrilled glass was doctor bladed with Platisol (Solaronix) and sintered at 450 °C for 15 min. The DSSCs were assembled using hot-melt sealing film (Solaronix). The composition of electrolyte was 0.1 M LiI, 0.05 M I$_2$, 0.6 M DMPII, and 0.5 M 4-*tert*-butyl pyridine (4-tBP) in acetonitrile. The electrolyte was injected into the assembled cells using Vac'n'Fill Syringe (Solaronix). The hole was covered by cover glass with hot-melt sealing film (Solaronix).

Solar Cell Characterization: The photocurrent–voltage (*J–V*) measurements were carried out on an Autolab potentiostat (Metrohm), driven by electrochemical software GPES, with class AAA SLB300A solar simulator (Sciencetech) as the light source at University of Edinburgh. The light intensity was calibrated to AM 1.5G (100 mW cm^{-2}) using a silicon reference cell. A black metal mask with a circular aperture of 0.0707 cm^2 was applied when measuring *J–V* curves. The EIS spectra of I$^-$/I$_3^-$ electrolyte-based devices setup was similar to the *J–V* measurements, except for using white LED as the light source and Frequency Response Analyser (FRA) software. The EIS spectra were recorded in the frequency range between 1 MHz and 0.1 Hz at various forward biases set to the corresponding voltage produced by white LED illumination. The obtained spectra were fit with a transmission line model[37] using Zview (Scribner Associates) software. IPCE measurements were conducted at University of Strathclyde. The IPCE of the solar cells were measured with a photospectrometer setup (Bentham PVE300) by illuminating the solar cell with modulated monochromatic light (Xenon and quartz halogen lamps) through 1.85 mm slit. The intensities of the lamps were calibrated with a silicon photodiode. The photospectrometer was operated in DC mode and the spectral resolution was set to 5 nm.

Supporting Information

Supporting Information is available from the Wiley Online Library or from the author.

Conflict of Interest

The authors declare no conflict of interest.

Data Availability Statement

The data that support the findings of this study are available from the corresponding author upon reasonable request.

[1] B. O'Regan, M. Grätzel, *Nature* **1991**, *353*, 737.

[2] M. K. Nazeeruddin, A. Kay, I. Rodicio, R. Humphry-Baker, E. Mueller, P. Liska, N. Vlachopoulos, M. Graetzel, *J. Am. Chem. Soc.* **1993**, *115*, 6382.

[3] M. K. Nazeeruddin, P. Péchy, T. Renouard, S. M. Zakeeruddin, R. Humphry-Baker, P. Cointe, P. Liska, L. Cevey, E. Costa,

V. Shklover, L. Spiccia, G. B. Deacon, C. A. Bignozzi, M. Grätzel, *J. Am. Chem. Soc.* **2001**, *123*, 1613.

[4] M. K. Nazeeruddin, F. De Angelis, S. Fantacci, A. Selloni, G. Viscardi, P. Liska, S. Ito, B. Takeru, M. Grätzel, *J. Am. Chem. Soc.* **2005**, *127*, 16835.

[5] A. Mishra, M. K. R. Fischer, P. Bäuerle, *Angew. Chem. Int. Ed.* **2009**, *48*, 2474.

[6] S. Zhang, X. Yang, Y. Numata, L. Han, *Energy Environ. Sci.* **2013**, *6*, 1443.

[7] A. Hagfeldt, G. Boschloo, L. Sun, L. Kloo, H. Pettersson, *Chem. Rev.* **2010**, *110*, 6595.

[8] V. Lee, *Org. Biomol. Chem.* **2019**, *17*, 9095.

[9] C. M. de L. Barbosa, F. M. Ferrão, J. B. Graceli, *Front. Endocrinol.* **2018**, *9*, 256.

[10] M. Liang, J. Chen, *Chem. Soc. Rev.* **2013**, *42*, 3453.

[11] E. Gabrielsson, H. Ellis, S. Feldt, H. Tian, G. Boschloo, A. Hagfeldt, L. Sun, *Adv. Energy Mater.* **2013**, *3*, 1647.

[12] W. Zeng, Y. Cao, Y. Bai, Y. Wang, Y. Shi, M. Zhang, F. Wang, C. Pan, P. Wang, *Chem. Mater.* **2010**, *22*, 1915.

[13] R. Li, J. Liu, N. Cai, M. Zhang, P. Wang, *J. Phys. Chem. B* **2010**, *114*, 4461.

[14] H. N. Tsao, C. Yi, T. Moehl, J.-H. Yum, S. M. Zakeeruddin, M. K. Nazeeruddin, M. Grätzel, *ChemSusChem* **2011**, *4*, 591.

[15] A. Yella, R. Humphry-Baker, B. F. E. Curchod, N. Ashari Astani, J. Teuscher, L. E. Polander, S. Mathew, J.-E. Moser, I. Tavernelli, U. Rothlisberger, M. Grätzel, M. K. Nazeeruddin, J. Frey, *Chem. Mater.* **2013**, *25*, 2733.

[16] G. Li, Y.-F. Zhou, X.-B. Cao, P. Bao, K.-J. Jiang, Y. Lin, L.-M. Yang, *Chem. Commun.* **2009**, 2201.

[17] J. M. Ji, H. Zhou, Y. K. Eom, C. H. Kim, H. K. Kim, *Adv. Energy Mater.* **2020**, *2000124*, 1.

[18] Z.-S. Huang, H. Meier, D. Cao, *J. Mater. Chem. C* **2016**, *4*, 2404.

[19] S. H. Kim, H. W. Kim, C. Sakong, J. Namgoong, S. W. Park, M. J. Ko, C. H. Lee, W. I. Lee, J. P. Kim, *Org. Lett.* **2011**, *13*, 5784.

[20] A. F. Buene, E. E. Ose, A. G. Zakariassen, A. Hagfeldt, B. H. Hoff, *J. Mater. Chem. A* **2019**, *7*, 7581.

[21] M. Marszalek, S. Nagane, A. Ichake, R. Humphry-Baker, V. Paul, S. M. Zakeeruddin, M. Grätzel, *J. Mater. Chem.* **2012**, *22*, 889.

[22] M.-H. Tsao, T.-Y. Wu, H.-P. Wang, I.-W. Sun, S.-G. Su, Y.-C. Lin, C.-W. Chang, *Mater. Lett.* **2011**, *65*, 583.

[23] H. Tian, X. Yang, R. Chen, Y. Pan, L. Li, A. Hagfeldt, L. Sun, *Chem. Commun.* **2007**, 3741.

[24] M. Marszalek, S. Nagane, A. Ichake, R. Humphry-Baker, V. Paul, S. M. Zakeeruddin, M. Grätzel, *RSC Adv.* **2013**, *3*, 7921.

[25] S. S. Soni, K. B. Fadadu, J. V. Vaghasiya, B. G. Solanki, K. K. Sonigara, A. Singh, D. Das, P. K. Iyer, *J. Mater. Chem. A* **2015**, *3*, 21664.

[26] R. M. El-Shishtawy, J.-D. Decoppet, F. A. M. Al-Zahrani, Y. Cao, S. B. Khan, M. S. Al-Ghamdi, B. G. Alhogbi, A. M. Asiri, S. M. Zakeeruddin, M. Grätzel, *New J. Chem.* **2018**, *42*, 9045.

[27] R. J. Barney, R. M. Richardson, D. F. Wiemer, *J. Org. Chem.* **2011**, *76*, 2875.

[28] H. Chen, Y. Gong, Á. Vázquez-Mayagoitia, J. Zhang, J. M. Cole, *ACS Appl. Energy Mater.* **2020**, *3*, 423.

[29] L. Zhang, J. M. Cole, *J. Mater. Chem. A* **2017**, *5*, 19541.

[30] G. Boschloo, *Front. Chem.* **2019**, *7*, 1.

[31] A. D. Becke, *J. Chem. Phys.* **1993**, *98*, 1372.

[32] T. Yanai, D. P. Tew, N. C. Handy, *Chem. Phys. Lett.* **2004**, *393*, 51.

[33] M. Caricato, G. W. Trucks, M. J. Frisch, K. B. Wiberg, *J. Chem. Theory Comput.* **2011**, *7*, 456.

[34] C.-J. Tan, C.-S. Yang, Y.-C. Sheng, H. W. Amini, H.-H. G. Tsai, *J. Phys. Chem. C* **2016**, *120*, 21272.

[35] Y. Xie, W. Wu, H. Zhu, J. Liu, W. Zhang, H. Tian, W.-H. Zhu, *Chem. Sci.* **2016**, *7*, 544.

[36] A. Hagfeldt, G. Boschloo, L. Sun, L. Kloo, H. Pettersson, *Energy Environ. Sci.* **2010**, *3*, 6595.

[37] F. Fabregat-Santiago, J. Bisquert, G. Garcia-Belmonte, G. Boschloo, A. Hagfeldt, *Sol. Energy Mater. Sol. Cells* **2005**, *87*, 117.

[38] F. Fabregat-Santiago, G. Garcia-Belmonte, I. Mora-Seró, J. Bisquert, *Phys. Chem. Chem. Phys.* **2011**, *13*, 9083.

[39] Y. Bai, J. Zhang, D. Zhou, Y. Wang, M. Zhang, P. Wang, *J. Am. Chem. Soc.* **2011**, *133*, 11442.

[40] Q. Wang, S. Ito, M. Grätzel, F. Fabregat-Santiago, I. Mora-Seró, J. Bisquert, T. Bessho, H. Imai, *J. Phys. Chem. B* **2006**, *110*, 25210.

[41] P. R. F. Barnes, K. Miettunen, X. Li, A. Y. Anderson, T. Bessho, M. Gratzel, B. C. O'Regan, *Adv. Mater.* **2013**, *25*, 1881.

[42] D. Zhou, Y. Bai, J. Zhang, N. Cai, M. Su, Y. Wang, M. Zhang, P. Wang, *J. Phys. Chem. C* **2011**, *115*, 816.

[43] S. Nakade, Y. Saito, W. Kubo, T. Kanzaki, T. Kitamura, Y. Wada, S. Yanagida, *Electrochem. commun.* **2003**, *5*, 804.

[44] S. R. Raga, E. M. Barea, F. Fabregat-Santiago, *J. Phys. Chem. Lett.* **2012**, *3*, 1629.

[45] D. Zhang, M. Stojanovic, Y. Ren, Y. Cao, F. T. Eickemeyer, E. Socie, N. Vlachopoulos, J.-E. Moser, S. M. Zakeeruddin, A. Hagfeldt, M. Grätzel, *Nat. Commun.* **2021**, *12*, 1777.

[46] M. Pazoki, U. B. Cappel, E. M. J. Johansson, A. Hagfeldt, G. Boschloo, *Energy Environ. Sci.* **2017**, *10*, 672.

[47] J. Preat, D. Jacquemin, E. A. Perpète, *Energy Environ. Sci.* **2010**, *3*, 891.

[48] Y. Ooyama, Y. Harima, *ChemPhysChem* **2012**, *13*, 4032.

[49] N. Koumura, Z. S. Wang, S. Mori, M. Miyashita, E. Suzuki, K. Hara, *J. Am. Chem. Soc.* **2006**, *128*, 14256.

[50] E. M. Barea, J. Bisquert, *Langmuir* **2013**, *29*, 8773.

[51] M. R. Maciejczyk, R. Chen, A. Brown, N. Zheng, N. Robertson, *J. Mater. Chem. C* **2019**, *7*, 8593.

[52] V. Leandri, J. Zhang, E. Mijangos, G. Boschloo, S. Ott, *J. Photochem. Photobiol. A Chem.* **2016**, *328*, 59.

[53] E. Tanaka, H. Michaels, M. Freitag, N. Robertson, *J. Mater. Chem. A* **2020**, *8*, 1279.

[54] M. D. Hanwell, D. E. Curtis, D. C. Lonie, T. Vandermeersch, E. Zurek, G. R. Hutchison, *J. Cheminform.* **2012**, *4*, 17.

[55] M. J. Frisch, G. W. Trucks, H. B. Schlegel, G. E. Scuseria, M. A. Robb, J. R. Cheeseman, G. Scalmani, V. Barone, B. Mennucci, G. A. Petersson, H. Nakatsuji, M. Caricato, X. Li, H. P. Hratchian, A. F. Izmaylov, J. Bloino, G. Zheng, J. L. Sonnenberg, M. Hada, M. Ehara, K. Toyota, R. Fukuda, J. Hasegawa, M. Ishida, T. Nakajima, Y. Honda, O. Kitao, H. Nakai, T. Vreven, J. Montgomery, et al., Gaussian, Inc., Wallingford, CT **2013**.

[56] M. Cossi, N. Rega, G. Scalmani, V. Barone, *J. Comput. Chem.* **2003**, *24*, 669.

[57] N. M. O'boyle, A. L. Tenderholt, K. M. Langner, *J. Comput. Chem.* **2008**, *29*, 839.

[58] R. Dennington, T. A. Keith, J. M. Millam, Semichem Inc., Shawnee Mission, KS **2016**.

[59] V. V. Pavlishchuk, A. W. Addison, *Inorg. Chim. Acta* **2000**, *298*, 97.

[60] B. Happ, D. Escudero, M. D. Hager, C. Friebe, A. Winter, H. Görls, E. Altuntaş, L. González, U. S. Schubert, *J. Org. Chem.* **2010**, *75*, 4025.